Single Image Super-Resolution via a Holistic Attention Network Supplementary Material

Ben Niu[1,⋆], Weilei Wen[2,⋆], Wenqi Ren[3], Xiangde Zhang[1], Lianping Yang[1,†], Shuzhen Wang[2], Kaihao Zhang[4], Xiaochun Cao[3,5], and Haifeng Shen[6]

[1] Northeastern University, Shenyang, China
[2] Xidian University, Xian, China
[3] SKLOIS, IIE, CAS
[4] Australian National University, Australia
[5] Peng Cheng Laboratory, Cyberspace Security Research Center, China
[6] AI Labs, Didi Chuxing, China

1 Overview

In this supplementary material, we first analyze the high-efficiency of the proposed HAN. Then we conduct two comparative trails between the proposed HAN and state-of-the-art SR methods on the low-resolution images with BI degradation and BD degradation in terms of model size and accuracy. Finally, we show more visual comparisons of various datasets [1,10,8,4,9] which contain both real-world images and down-sampled images.

2 Analysis of Model Parameters

The high-quality results of the proposed model are attributed to the global enhanced features obtained by the holistic attention model. Although we use RCAN as the backbone of our model, the parameters do not increase too many as shown in Figure 1 and 2. These results demonstrate that our proposed HAN can obtain a better trade-off between the performance and model complexity.

2.1 Analysis of the HAN Performance on BI Degradation

As shown in Figure 1, we can make a comparison of model size and performance of different SR reconstruction networks. Among all the networks shown in the figure, our HAN performs best and achieves 31.42 dB on the Manga109 dataset with 4× SR, which is 0.3 dB higher than the recent work of RCAN, and the parameter amount is only 16.1M.

⋆ Equal contribution
† Corresponding author

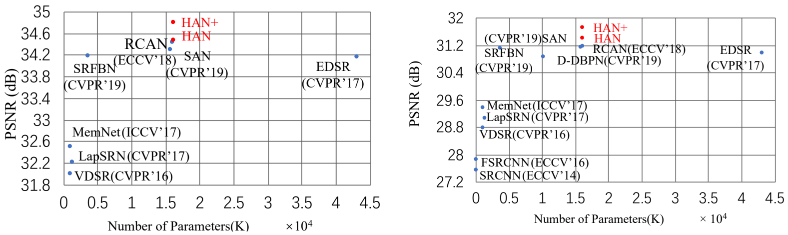

(a) Results on Manga109 (3×) (b) Results on Manga109 (4×)

Fig. 1. Performance and number of parameters. Results are evaluated on Manga109

2.2 Analysis of the HAN Performance on BD Degradation

In addition to experiment on BI degradation, we further conduct a comparison of model size and performance of different SR networks on BD degradation in Figure 2. As shown, our method achieves best result among all of these state-of-the-art algorithms, which demonstrate the robustness of our proposed HAN on both BI and BD degradations.

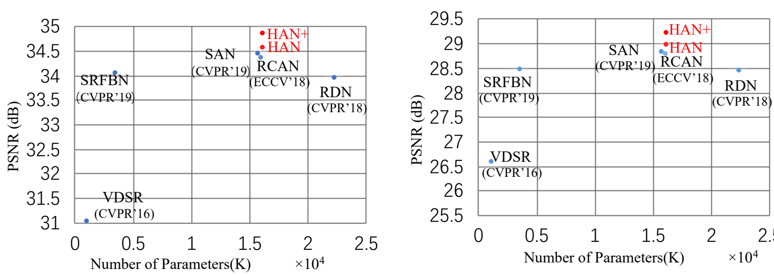

(a) on Manga109 (3×) (b) on Urban109 (3×)

Fig. 2. Performance and number of parameters. are evaluated on the Manga109 [9] and the Urban100 with BD degradation model

3 More Qualitative Comparisons

In this section, we present more qualitative comparisons and compare our method against several state-of-the-art super-resolution methods.

Specifically, we show visual comparisons of various methods on the Urban100 [4] and BSDS100 [8] datasets for 3× and 4× SR in Figure 3-15 and Figure 16-25, respectively. Then, Figure 26-32 show the challenging examples for 8× SR on the Urban100 dataset.

Finally, we demonstrate an application of super-resolving real-world photographs with JPEG compression artifacts of the proposed method. In these cases, the ground-truth images are available. As shown in Figure 33-37, our algorithm can reconstruct sharper and more accurate images than the state-of-the-art SR approaches.

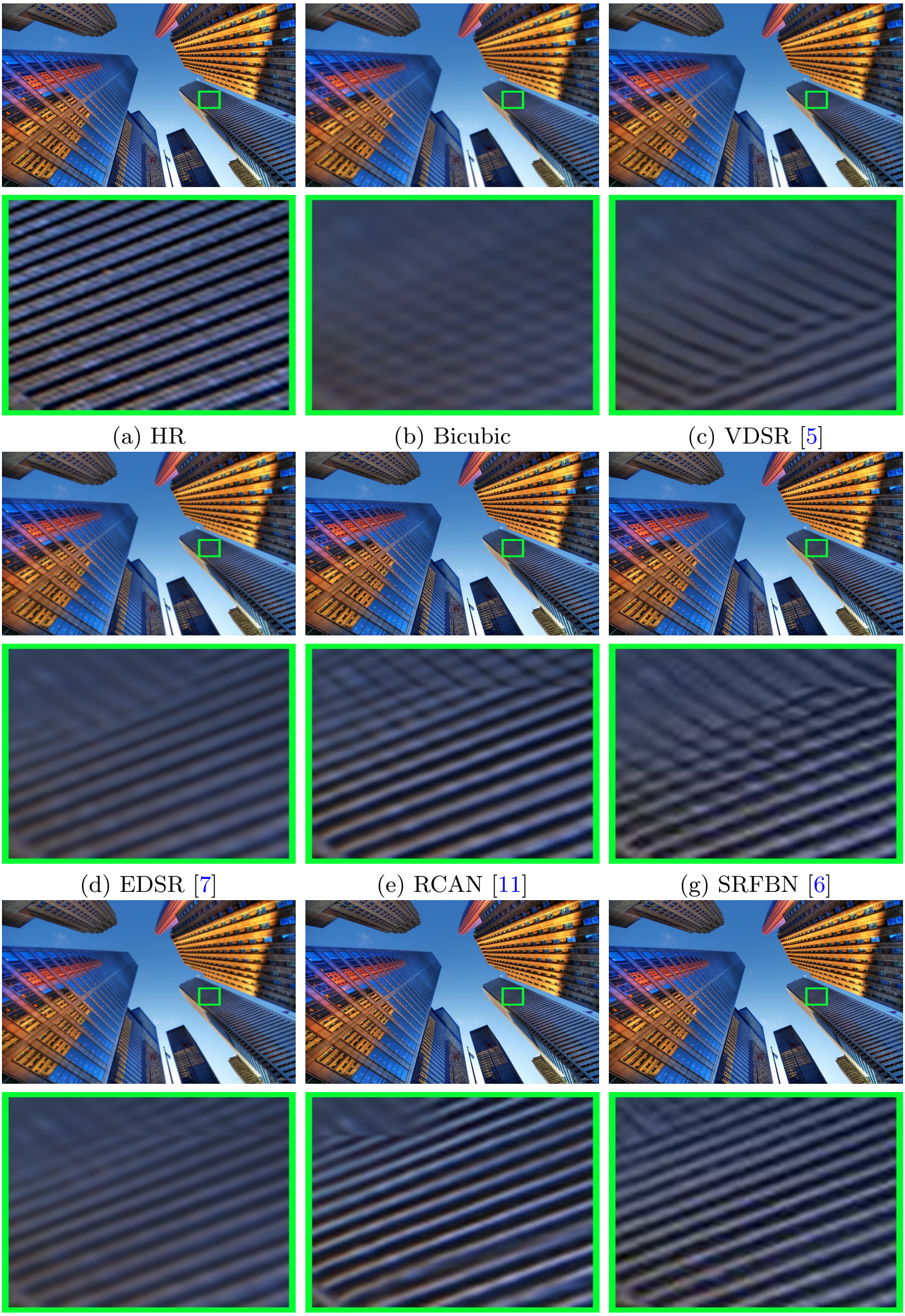

(a) HR (b) Bicubic (c) VDSR [5]

(d) EDSR [7] (e) RCAN [11] (g) SRFBN [6]

(h) SAN [2] (i) HAN(our) (j) HAN+(our)

Fig. 3. Visual comparison for 3× SR with BD model on the Urban100 dataset

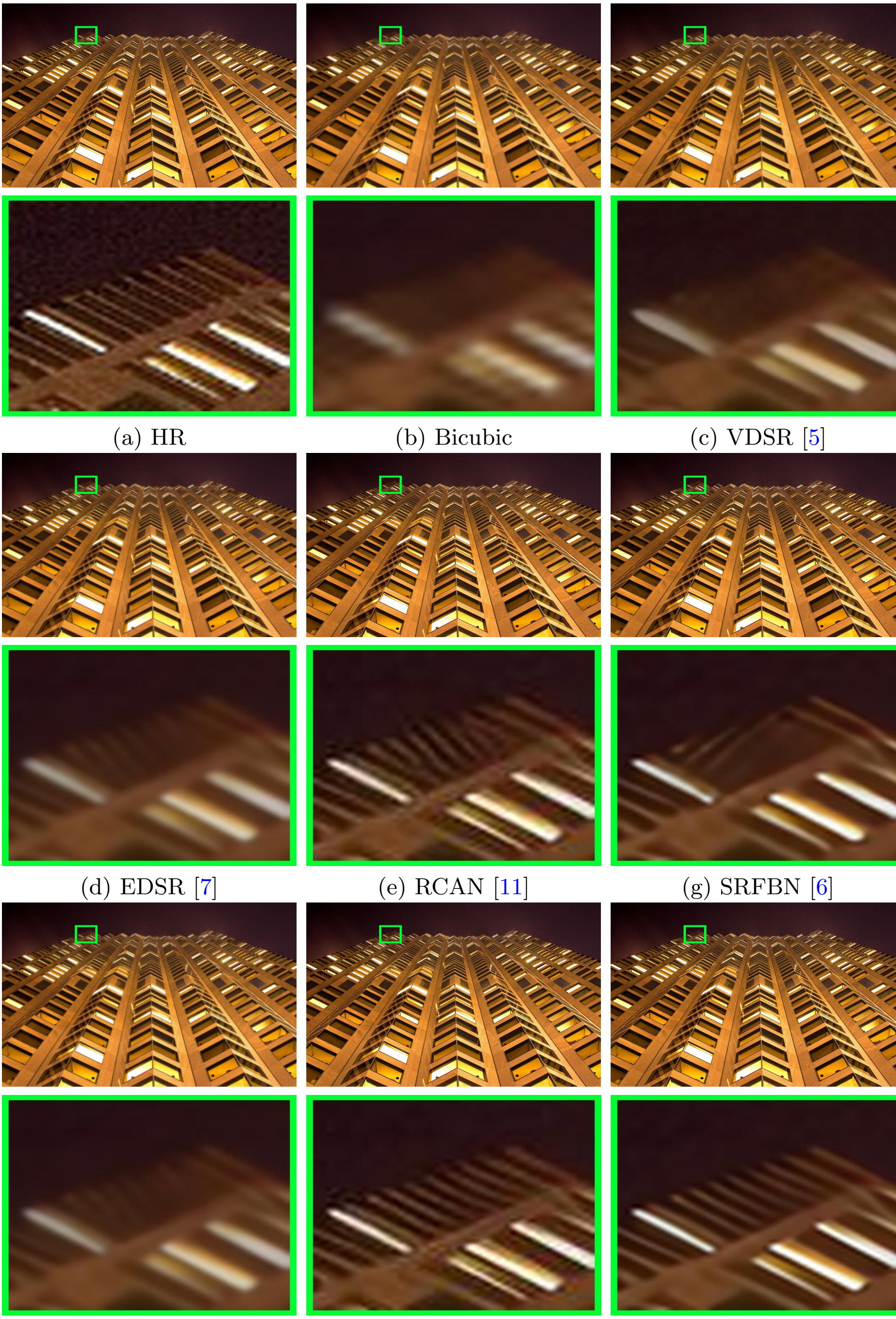

(a) HR (b) Bicubic (c) VDSR [5]

(d) EDSR [7] (e) RCAN [11] (g) SRFBN [6]

(h) SAN [2] (i) HAN(our) (j) HAN+(our)

Fig. 4. Visual comparison for 3× SR with BD model on the Urban100 dataset

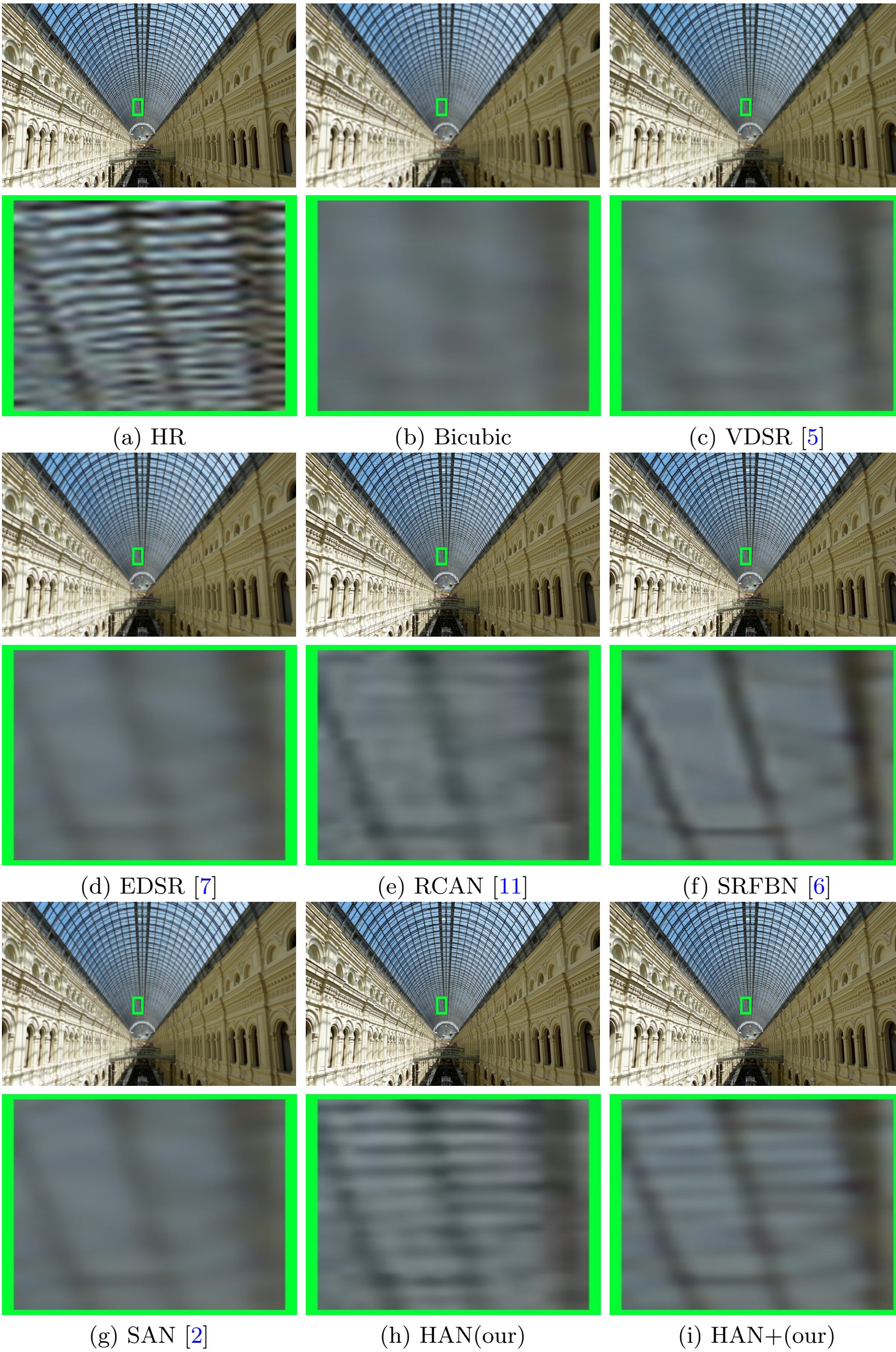

(a) HR (b) Bicubic (c) VDSR [5]

(d) EDSR [7] (e) RCAN [11] (f) SRFBN [6]

(g) SAN [2] (h) HAN(our) (i) HAN+(our)

Fig. 5. Visual comparison for 3× SR with BD model on the Urban100 dataset

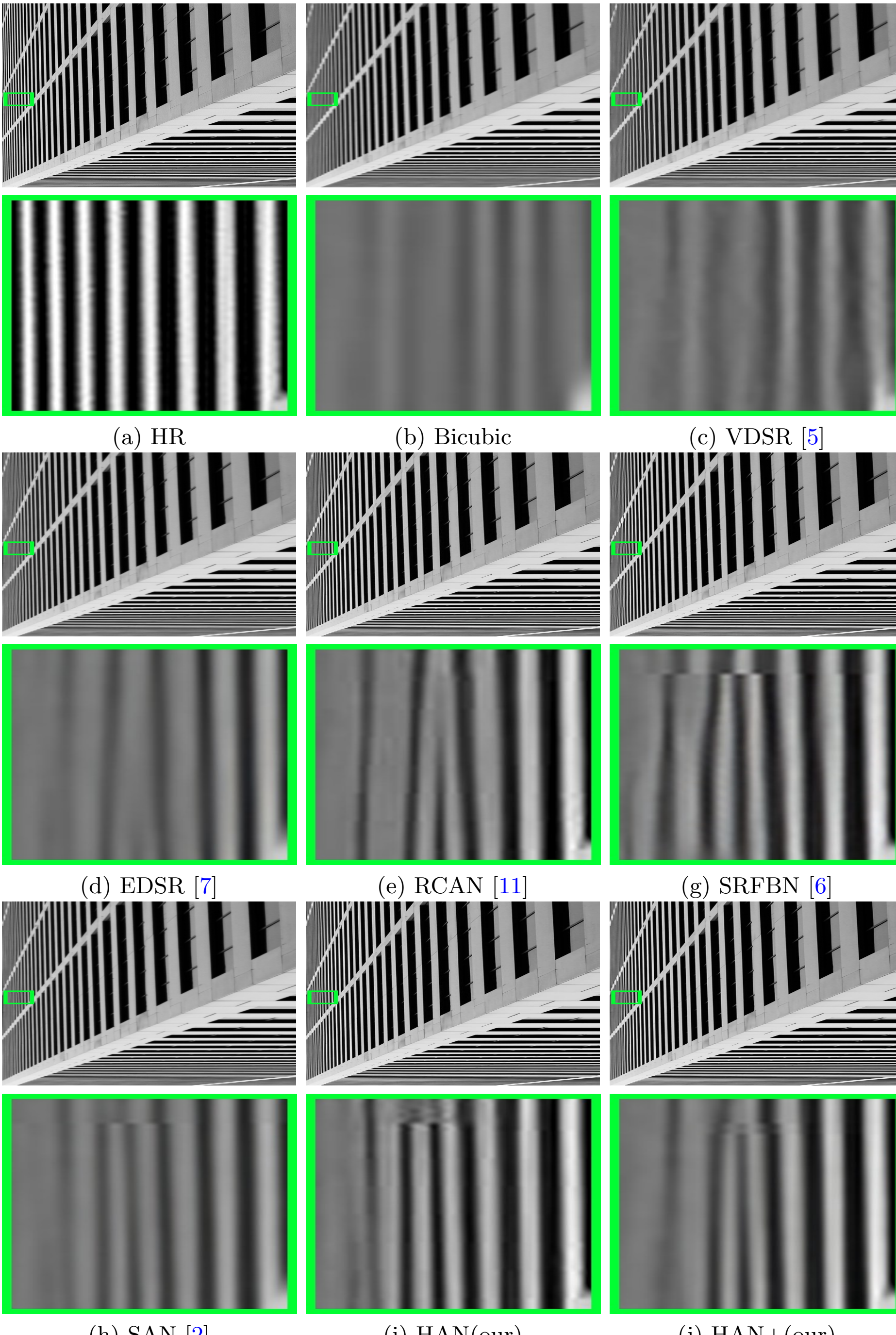

(a) HR (b) Bicubic (c) VDSR [5]

(d) EDSR [7] (e) RCAN [11] (g) SRFBN [6]

(h) SAN [2] (i) HAN(our) (j) HAN+(our)

Fig. 6. Visual comparison for 3× SR with BD model on the Urban100 dataset

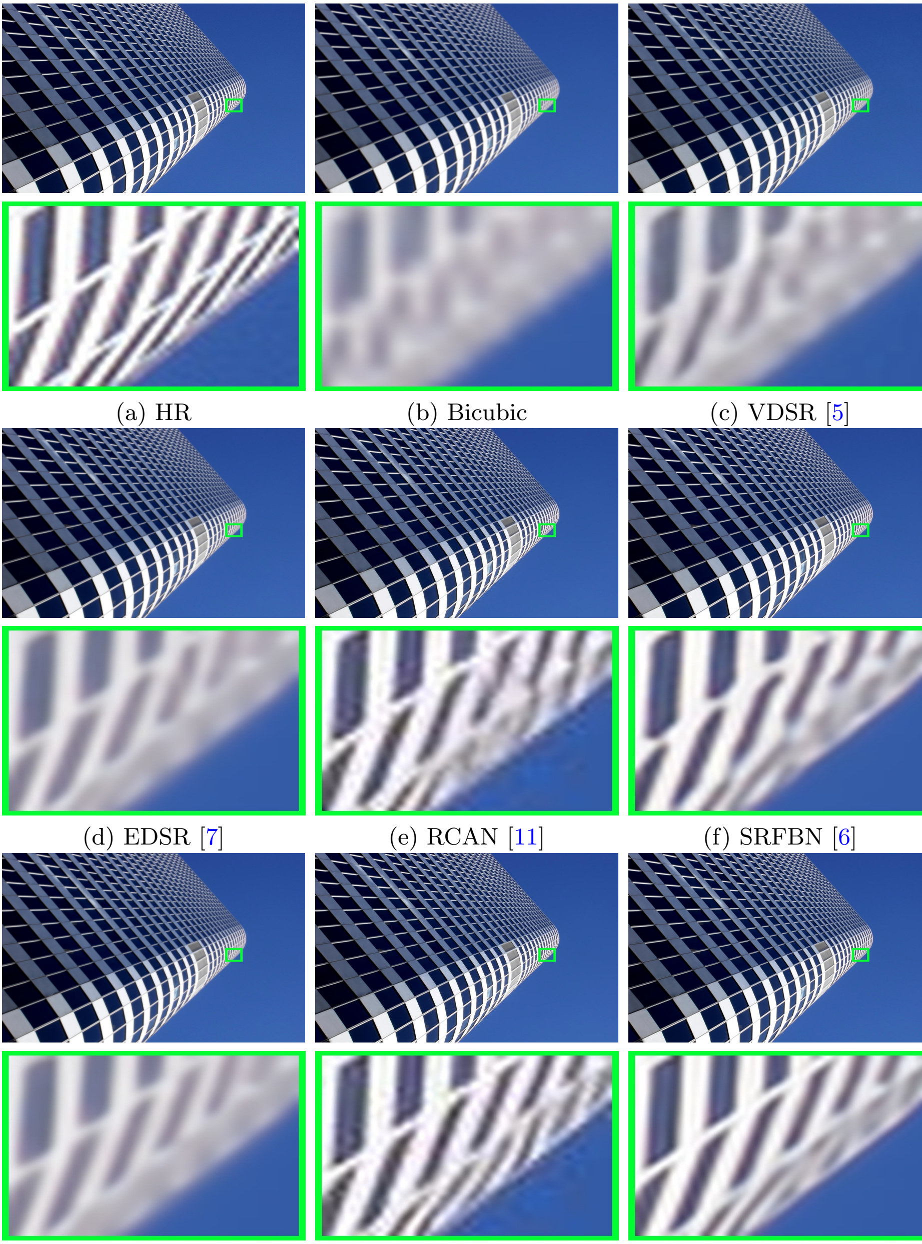

(a) HR (b) Bicubic (c) VDSR [5]
(d) EDSR [7] (e) RCAN [11] (f) SRFBN [6]
(g) SAN [2] (h) HAN(our) (i) HAN+(our)

Fig. 7. Visual comparison for 3× SR with BD model on the Urban100 dataset

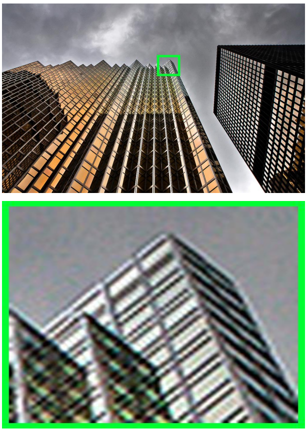

(a) HR

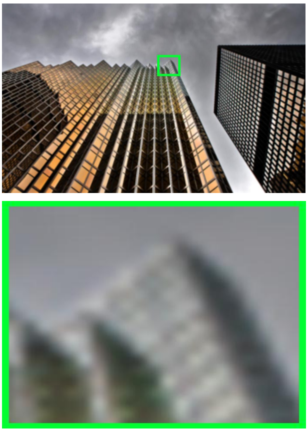

(b) Bicubic

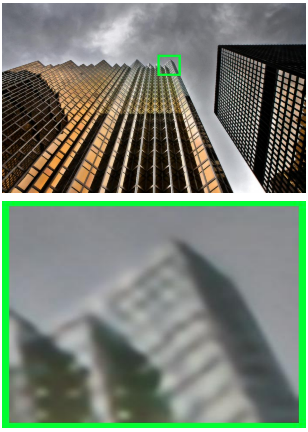

(c) VDSR [5]

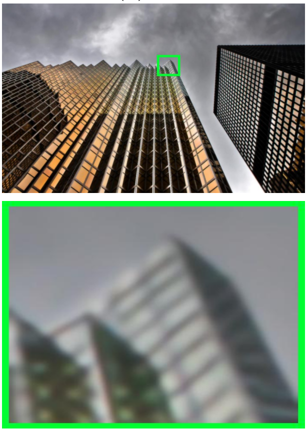

(d) EDSR [7]

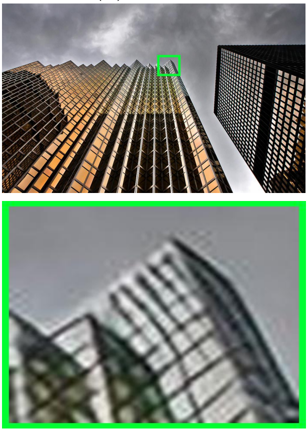

(e) RCAN [11]

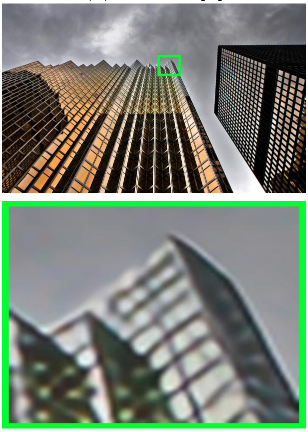

(g) SRFBN [6]

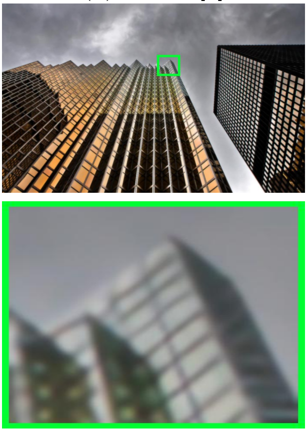

(h) SAN [2]

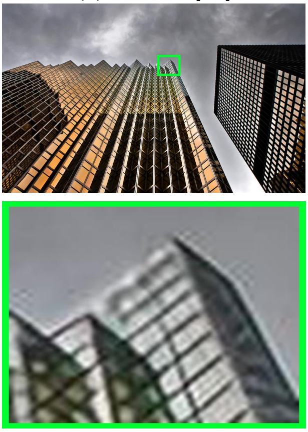

(i) HAN(our)

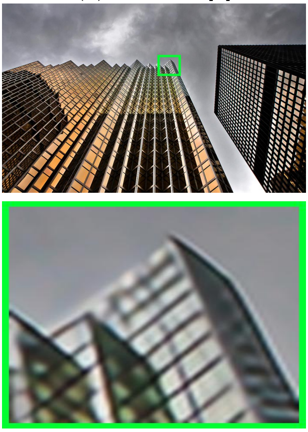

(j) HAN+(our)

Fig. 8. Visual comparison for 3× SR with BD model on the Urban100 dataset

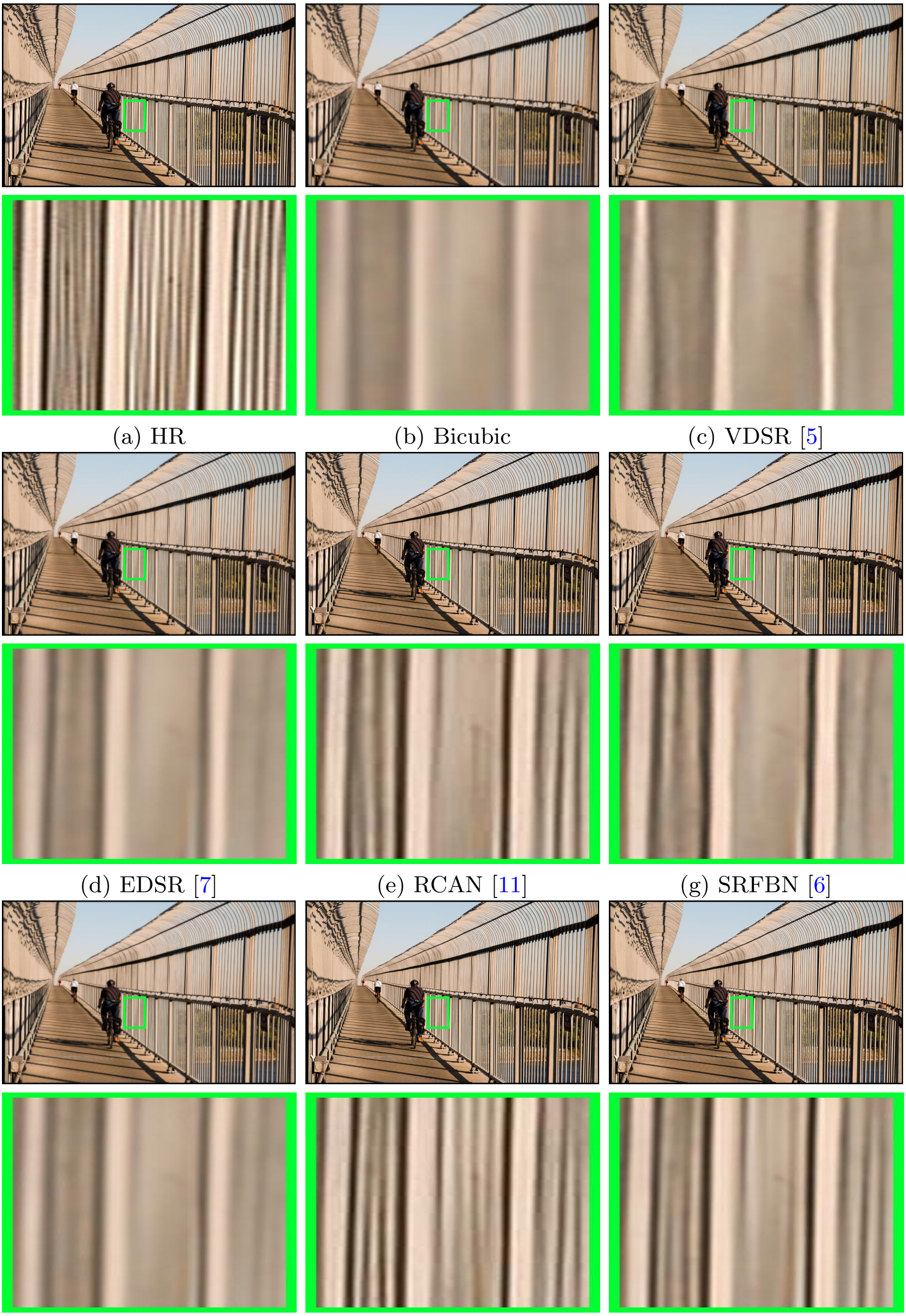

(a) HR (b) Bicubic (c) VDSR [5]

(d) EDSR [7] (e) RCAN [11] (g) SRFBN [6]

(h) SAN [2] (i) HAN(our) (j) HAN+(our)

Fig. 9. Visual comparison for 3× SR with BD model on the Urban100 dataset

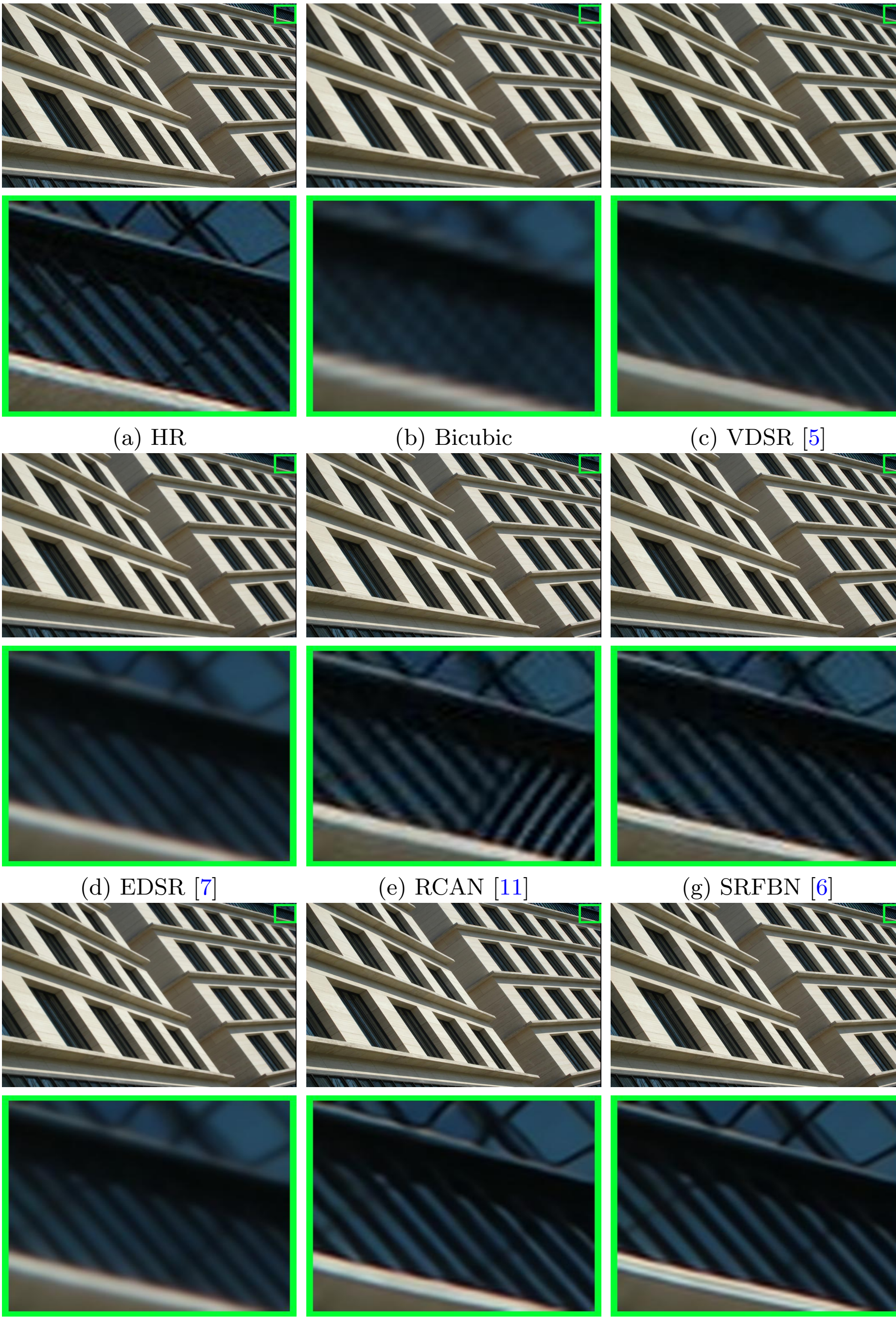

(a) HR (b) Bicubic (c) VDSR [5]

(d) EDSR [7] (e) RCAN [11] (g) SRFBN [6]

(h) SAN [2] (i) HAN(our) (j) HAN+(our)

Fig. 10. Visual comparison for 3× SR with BD model on the Urban100 dataset

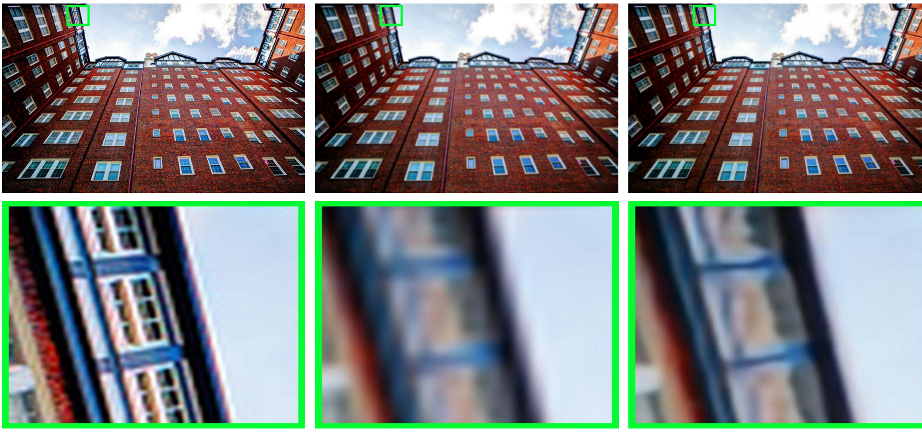

(a) HR (b) Bicubic (c) VDSR [5]

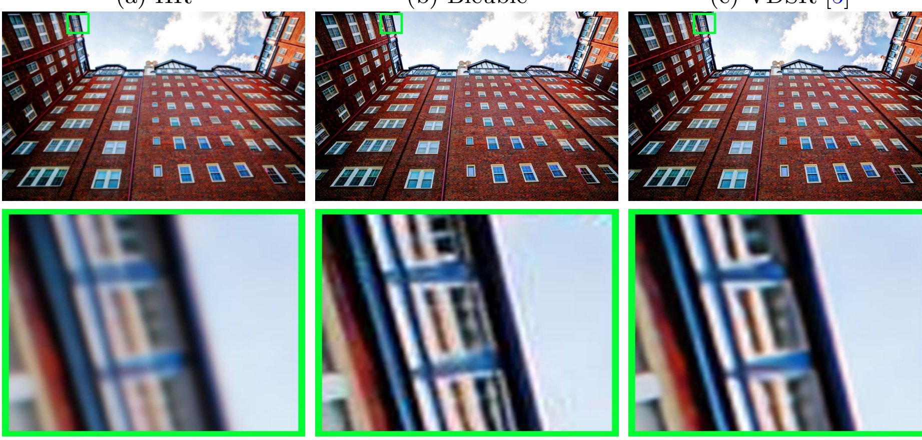

(d) EDSR [7] (e) RCAN [11] (g) SRFBN [6]

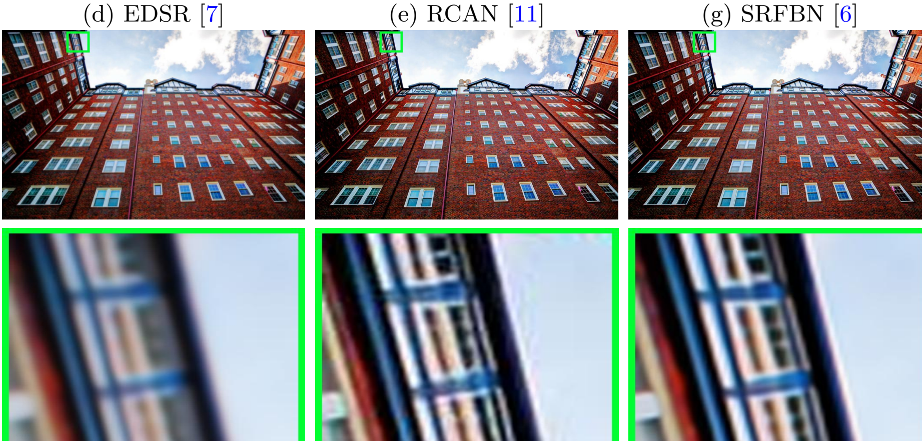

(h) SAN [2] (i) HAN(our) (j) HAN+(our)

Fig. 11. Visual comparison for 3× SR with BD model on the Urban100 dataset

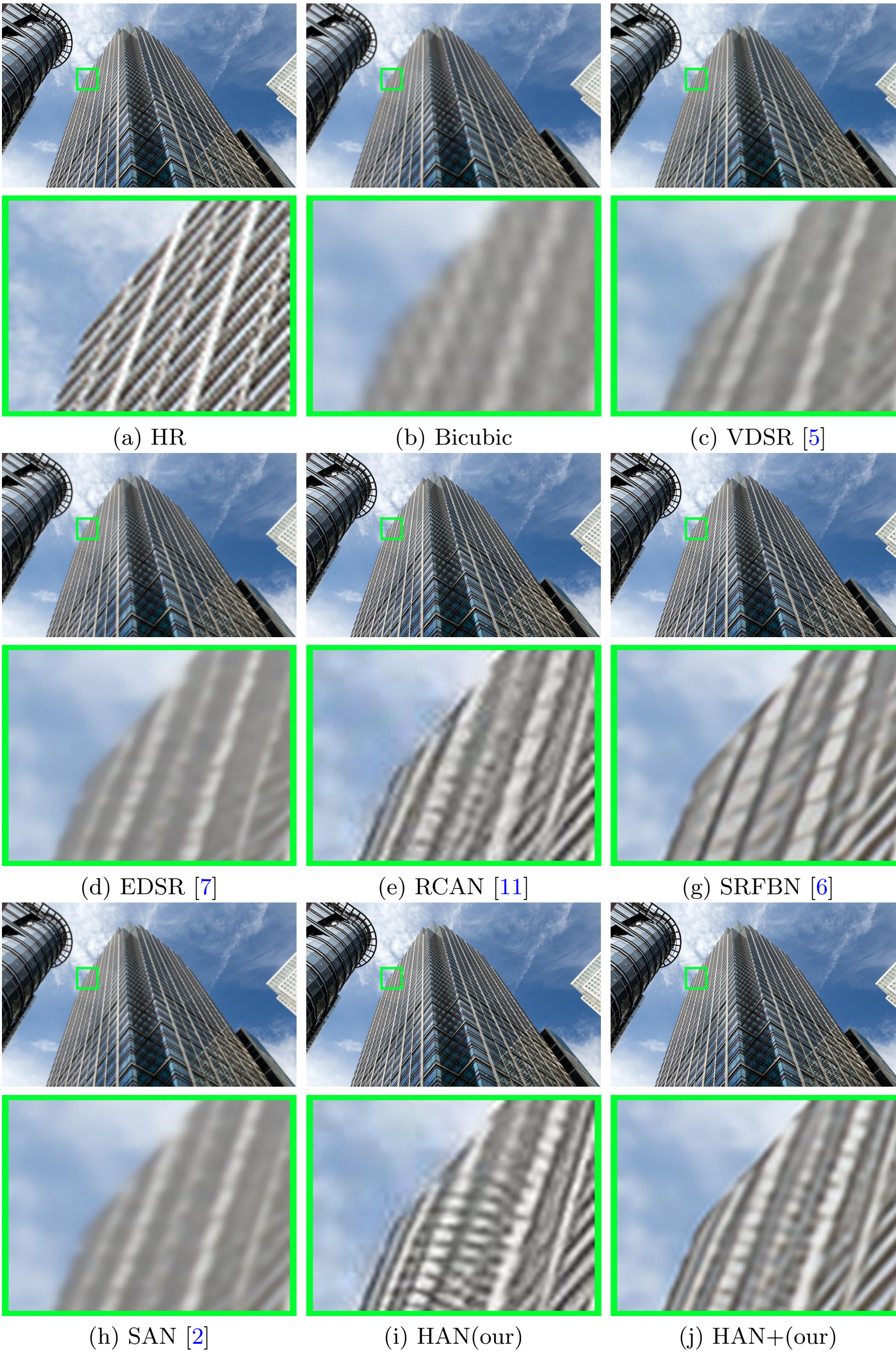

Fig. 12. Visual comparison for 3× SR with BD model on the Urban100 dataset

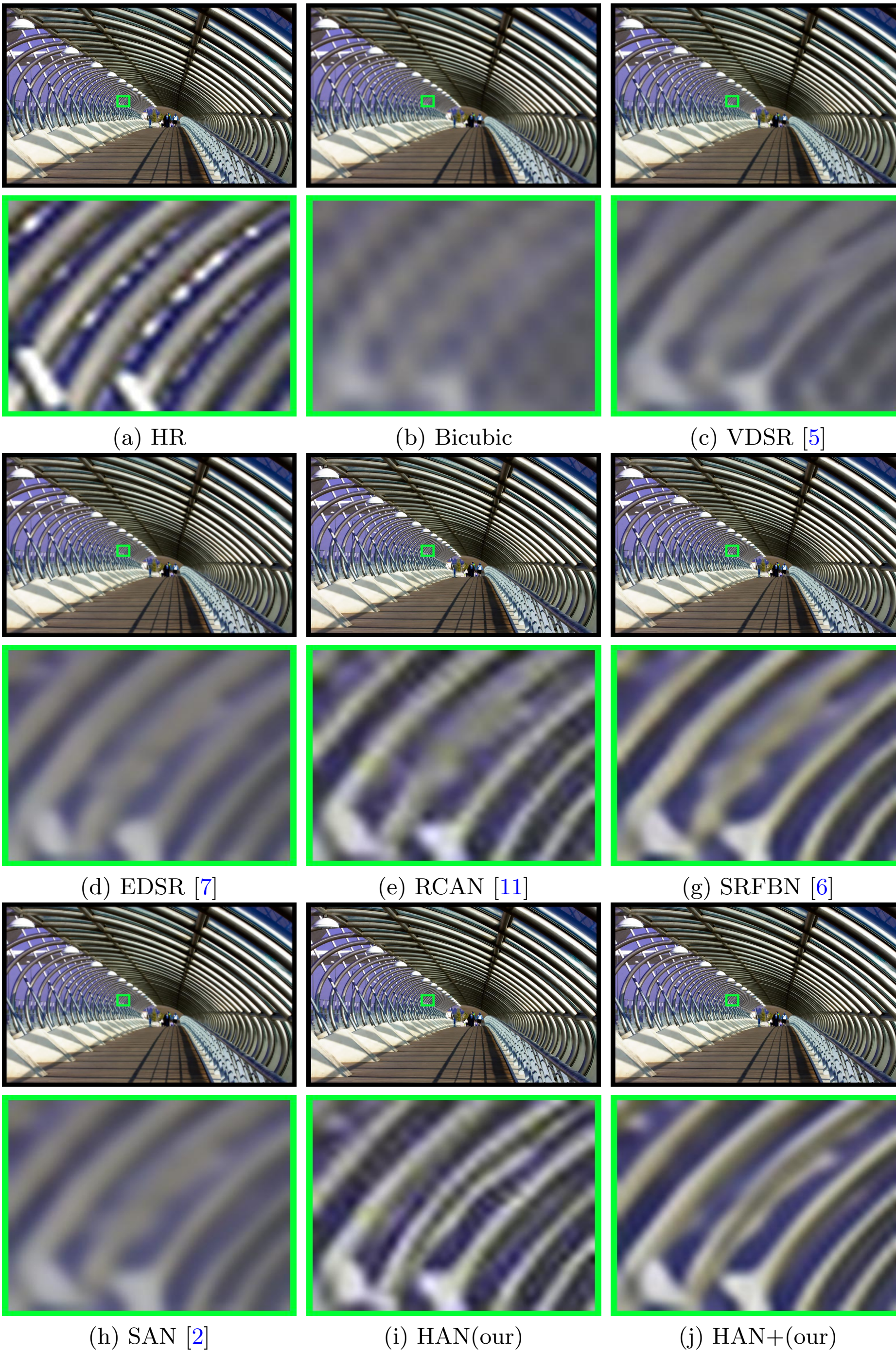

Fig. 13. Visual comparison for 3× SR with BD model on the Urban100 dataset

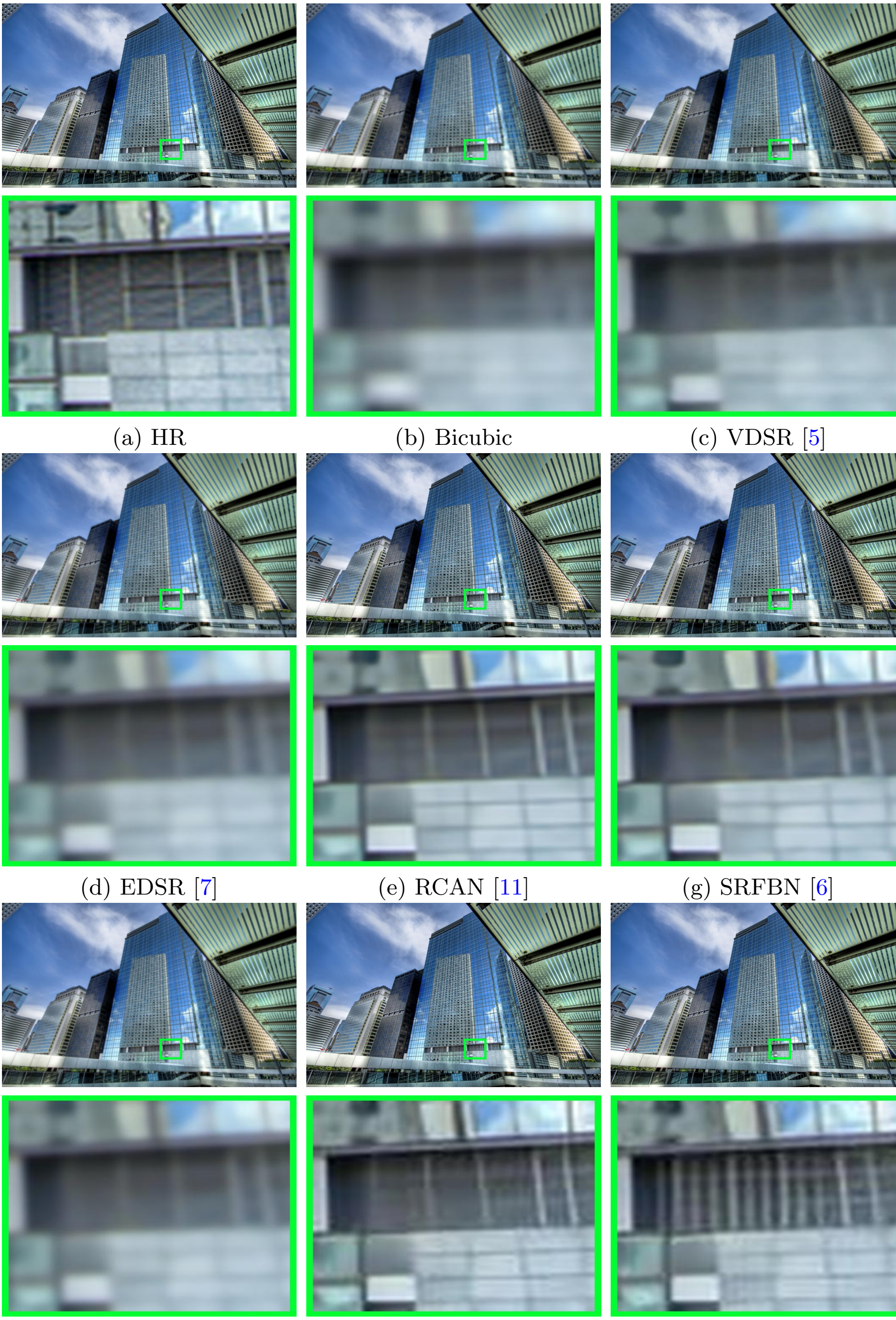

(a) HR (b) Bicubic (c) VDSR [5]

(d) EDSR [7] (e) RCAN [11] (g) SRFBN [6]

(h) SAN [2] (i) HAN(our) (j) HAN+(our)

Fig. 14. Visual comparison for 3× SR with BD model on the Urban100 dataset

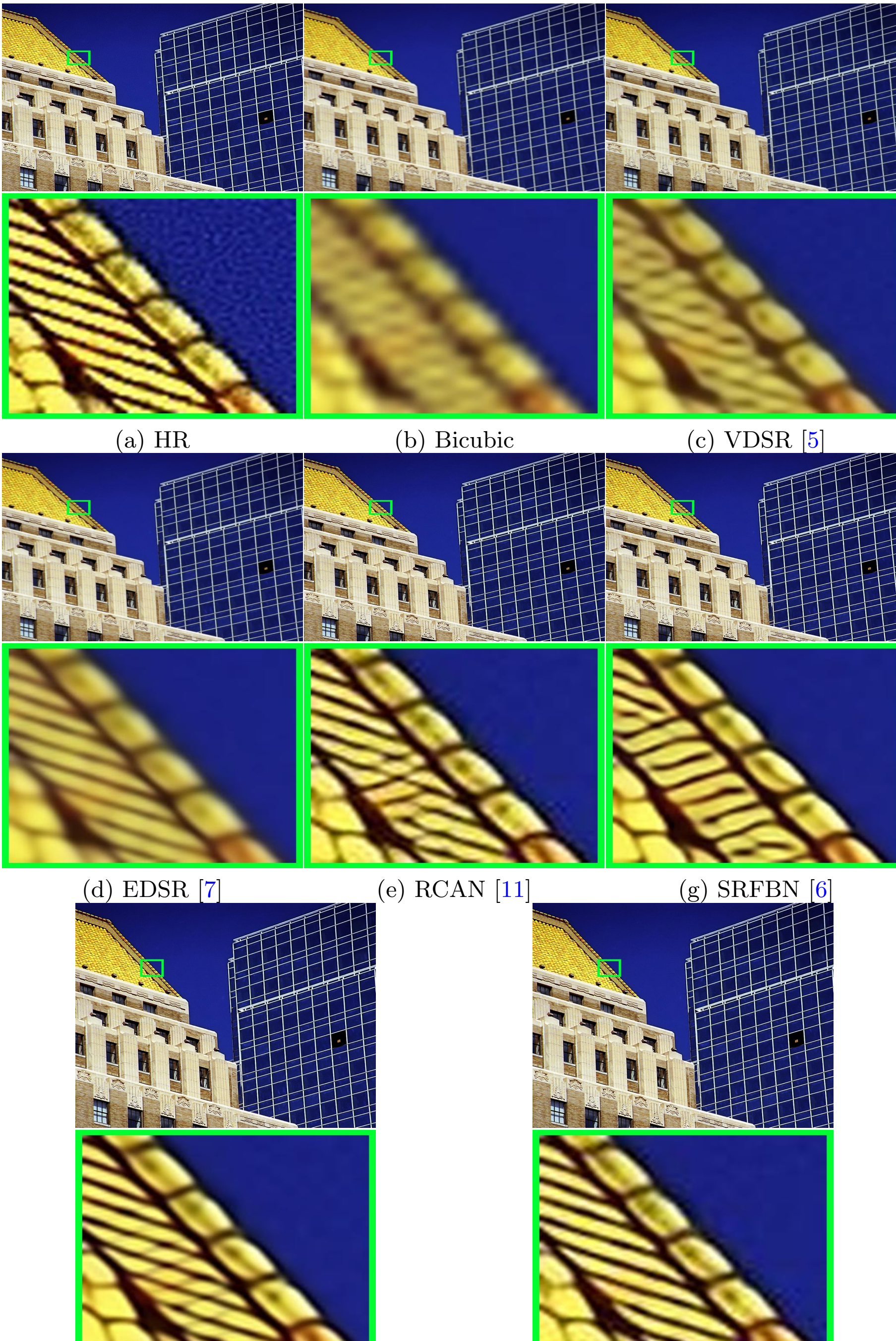

(a) HR (b) Bicubic (c) VDSR [5]

(d) EDSR [7] (e) RCAN [11] (g) SRFBN [6]

(h) HAN(our) (i) HAN+(our)

Fig. 15. Visual comparison for 3× SR with BD model on the Urban100 dataset

(a) HR (b) Bicubic (c) VDSR [5]
(d) EDSR [7] (e)RDN [12] (f)RCAN [11]
(g) SRFBN [6] (h) SAN [2] (i) HAN(our)

Fig. 16. Visual comparison for 4× SR on the BSDS100 dataset

(a) HR (b) Bicubic (c) VDSR [5]

(d) EDSR [7] (e)RDN [12] (f)RCAN [11]

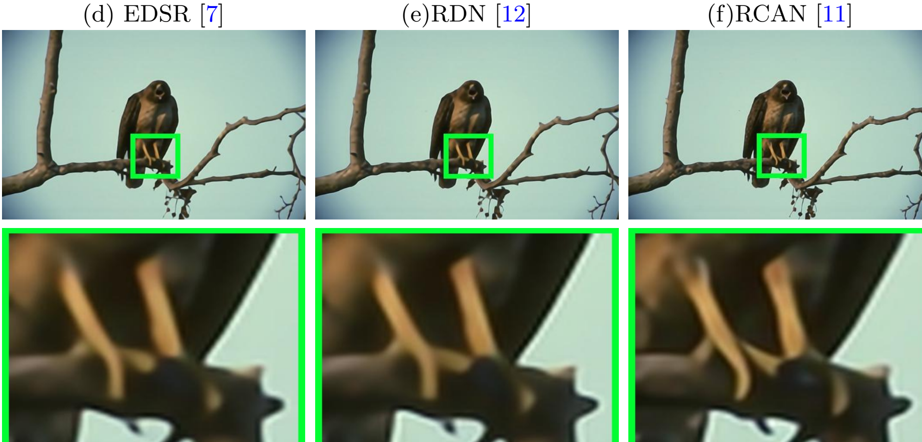

(g) SRFBN [6] (h) SAN [2] (i) HAN(our)

Fig. 17. Visual comparison for 4× SR on the BSDS100 dataset

(a) HR (b) Bicubic (c) VDSR [5]

(d) EDSR [7] (e)RDN [12] (f)RCAN [11]

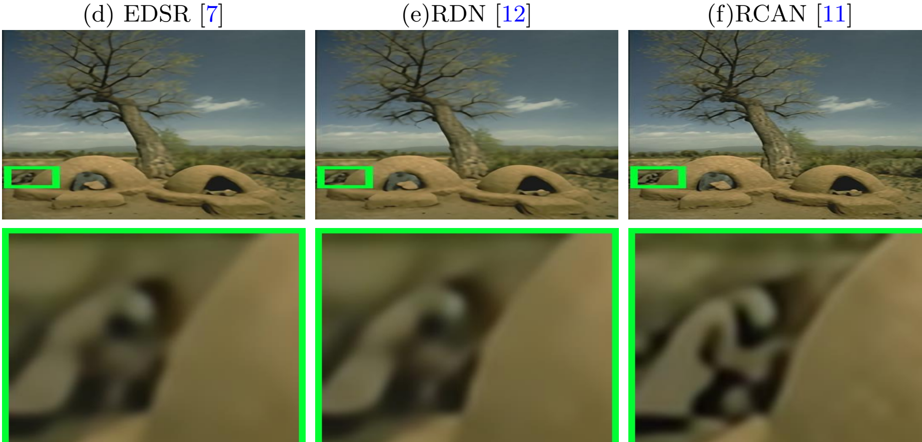

(g) SRFBN [6] (h) SAN [2] (i) HAN(our)

Fig. 18. Visual comparison for 4× SR on the BSDS100 dataset

(a) HR (b) Bicubic (c) VDSR [5]

(d) EDSR [7] (e)RDN [12] (f)RCAN [11]

(g) SRFBN [6] (h) SAN [2] (i) HAN(our)

Fig. 19. Visual comparison for 4× SR on the BSDS100 dataset

(a) HR (b) Bicubic (c) VDSR [5]

(d) EDSR [7] (e)RDN [12] (f)RCAN [11]

(g) SRFBN [6] (h) SAN [2] (i) HAN(our)

Fig. 20. Visual comparison for 4× SR on the BSDS100 dataset

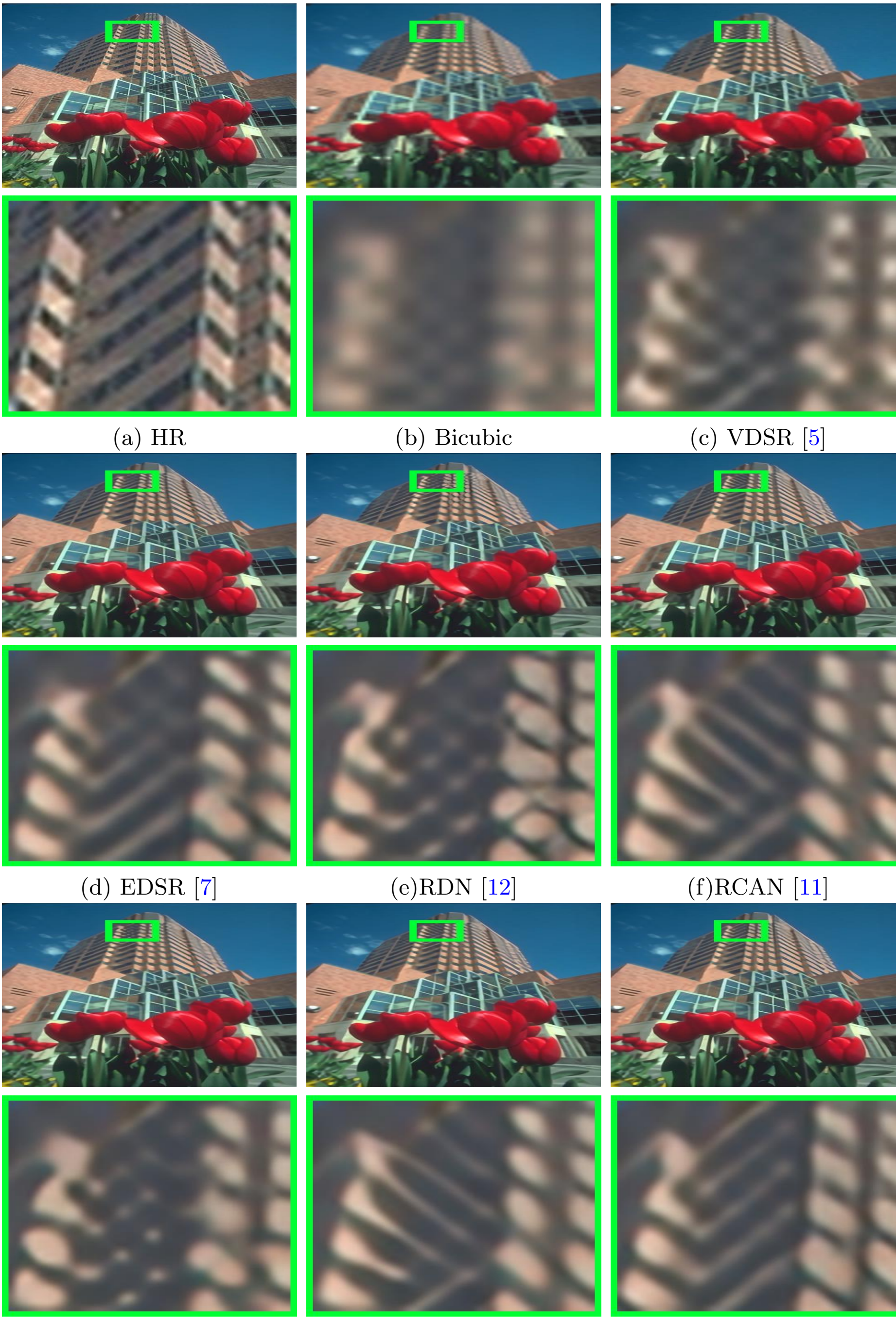

(a) HR (b) Bicubic (c) VDSR [5]

(d) EDSR [7] (e)RDN [12] (f)RCAN [11]

(g) SRFBN [6] (h) SAN [2] (i) HAN(our)

Fig. 21. Visual comparison for 4× SR on the BSDS100 dataset

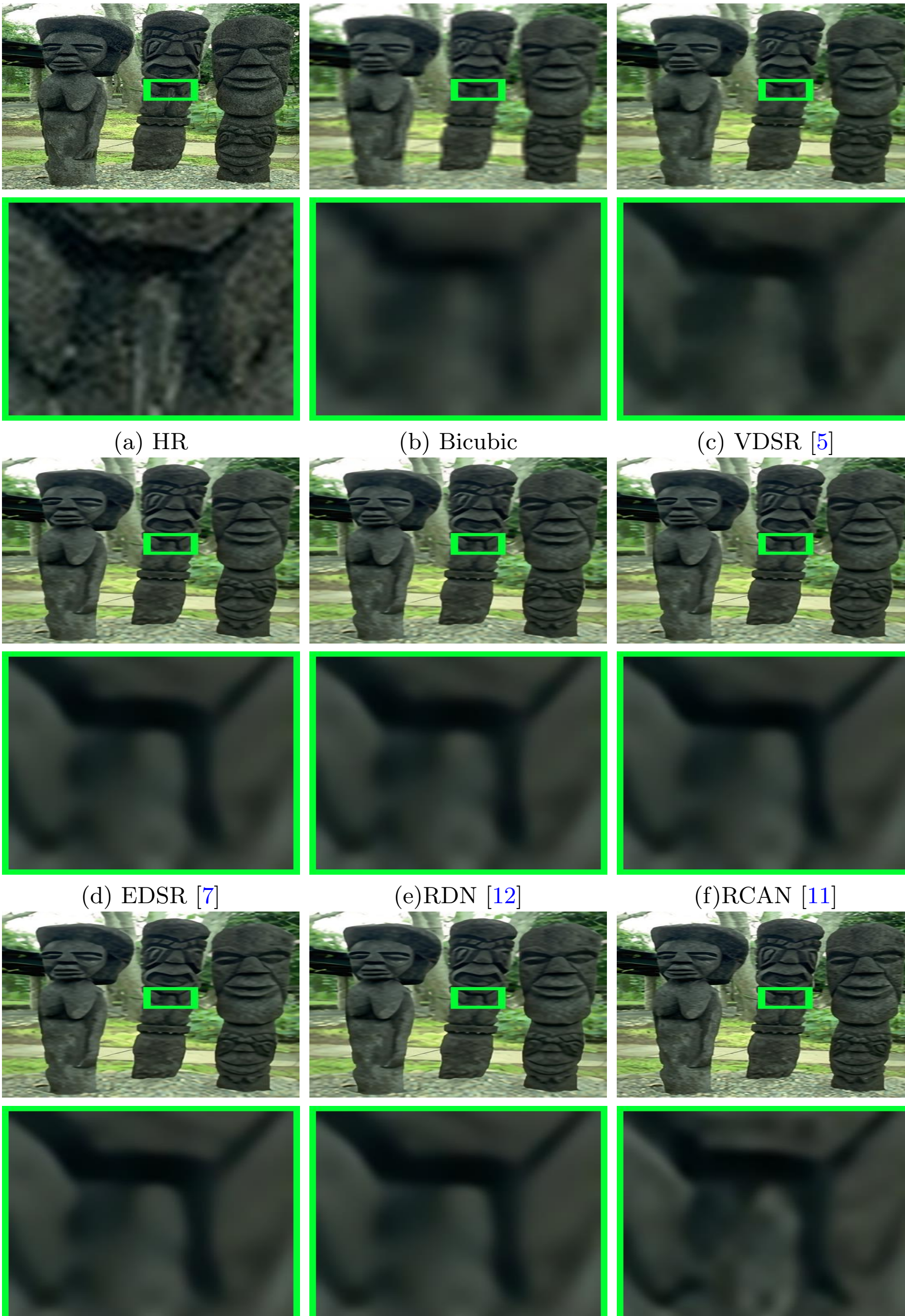

(a) HR (b) Bicubic (c) VDSR [5]

(d) EDSR [7] (e)RDN [12] (f)RCAN [11]

(g) SRFBN [6] (h) SAN [2] (i) HAN(our)

Fig. 22. Visual comparison for 4× SR on the BSDS100 dataset

(a) HR (b) Bicubic (c) VDSR [5]

(d) EDSR [7] (e)RDN [12] (f)RCAN [11]

(g) SRFBN [6] (h) SAN [2] (i) HAN(our)

Fig. 23. Visual comparison for 4× SR on the BSDS100 dataset

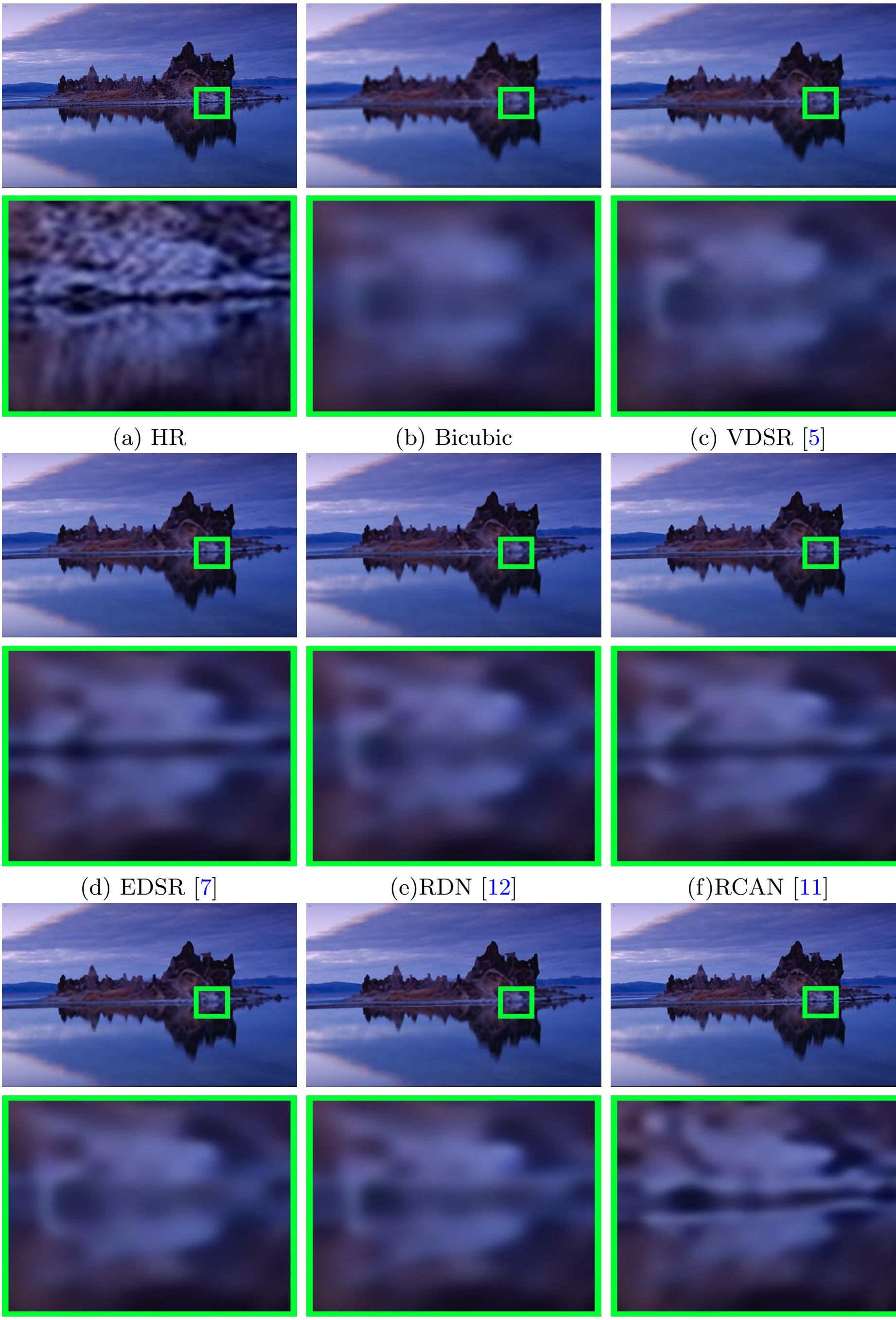

(a) HR (b) Bicubic (c) VDSR [5]

(d) EDSR [7] (e)RDN [12] (f)RCAN [11]

(g) SRFBN [6] (h) SAN [2] (i) HAN(our)

Fig. 24. Visual comparison for 4× SR on the BSDS100 dataset

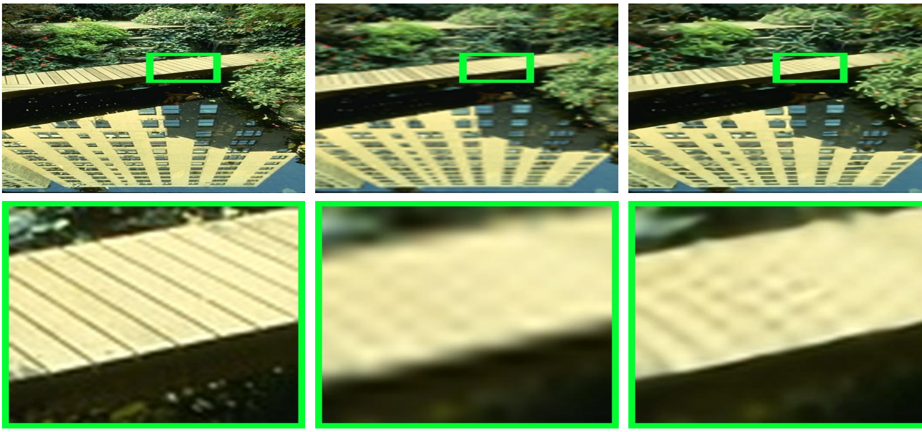

(a) HR (b) Bicubic (c) VDSR [5]

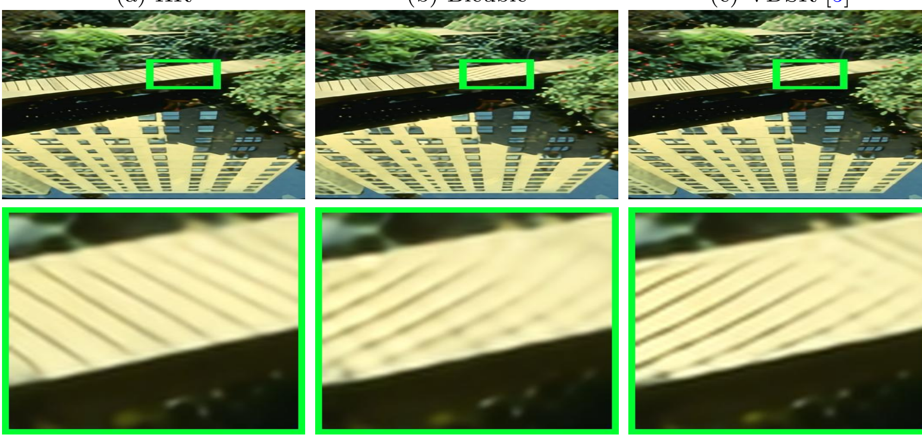

(d) EDSR [7] (e)RDN [12] (f)RCAN [11]

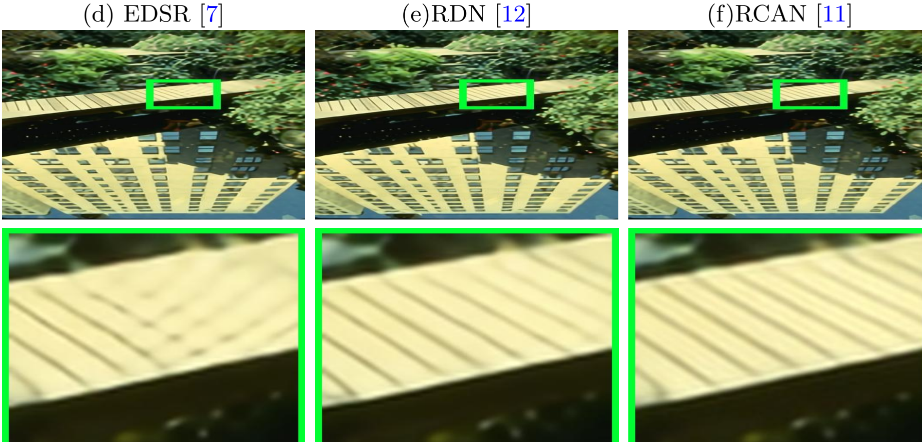

(g) SRFBN [6] (h) SAN [2] (i) HAN(our)

Fig. 25. Visual comparison for 4× SR on the BSDS100 dataset

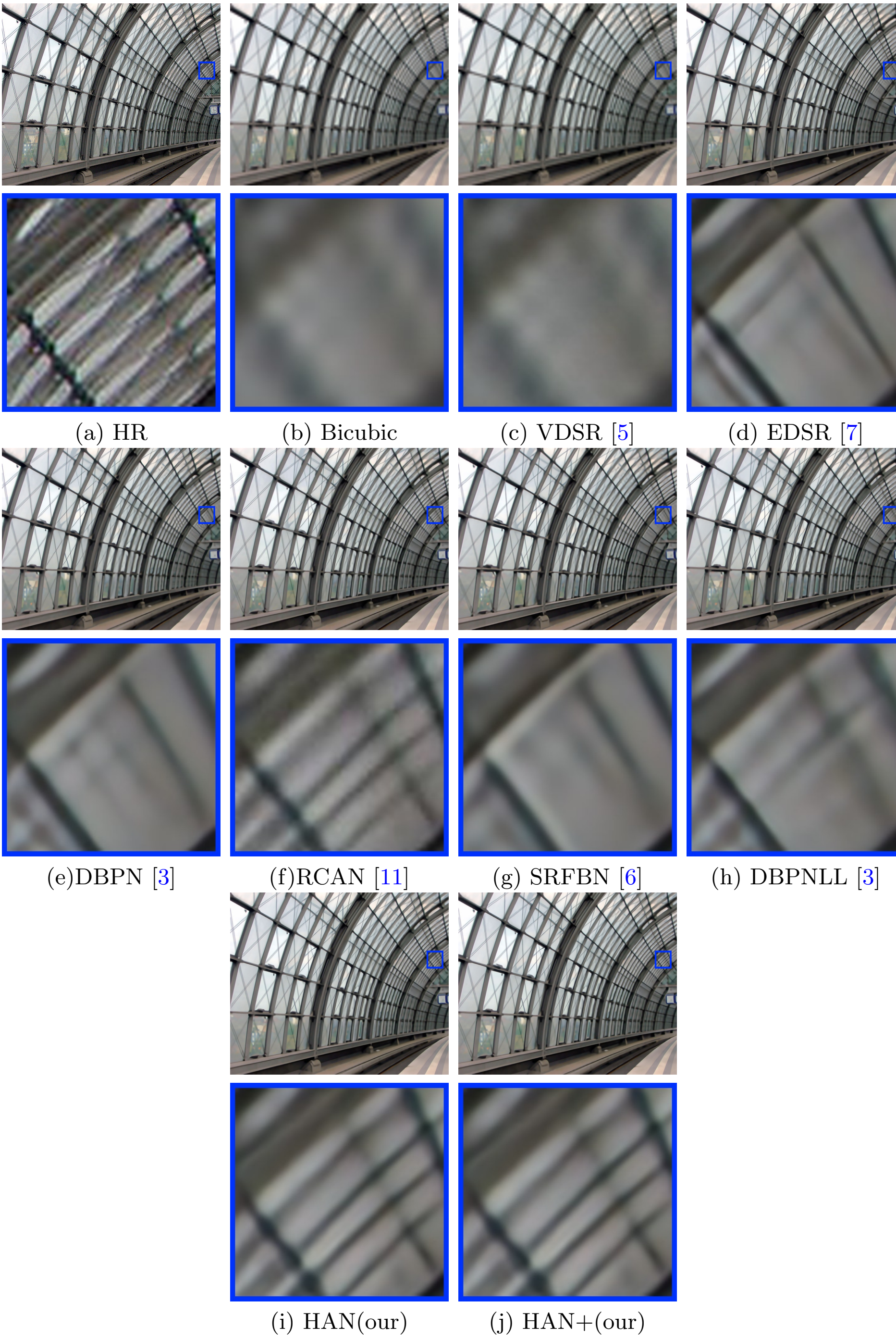

Fig. 26. Visual comparison for 8× SR on the Urban100 dataset

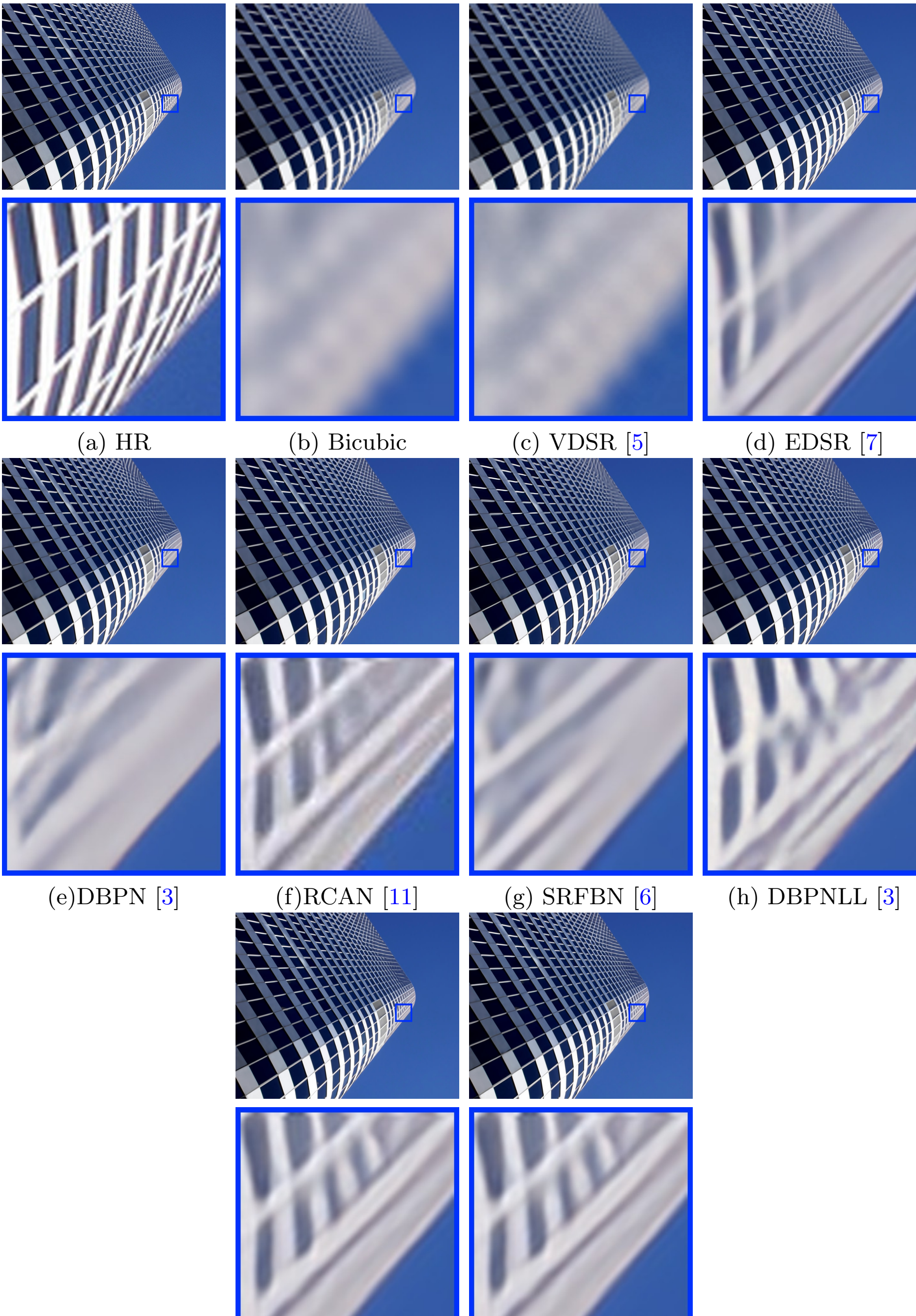

(a) HR (b) Bicubic (c) VDSR [5] (d) EDSR [7]

(e)DBPN [3] (f)RCAN [11] (g) SRFBN [6] (h) DBPNLL [3]

(i) HAN(our) (j) HAN+(our)

Fig. 27. Visual comparison for 8× SR on the Urban100 dataset

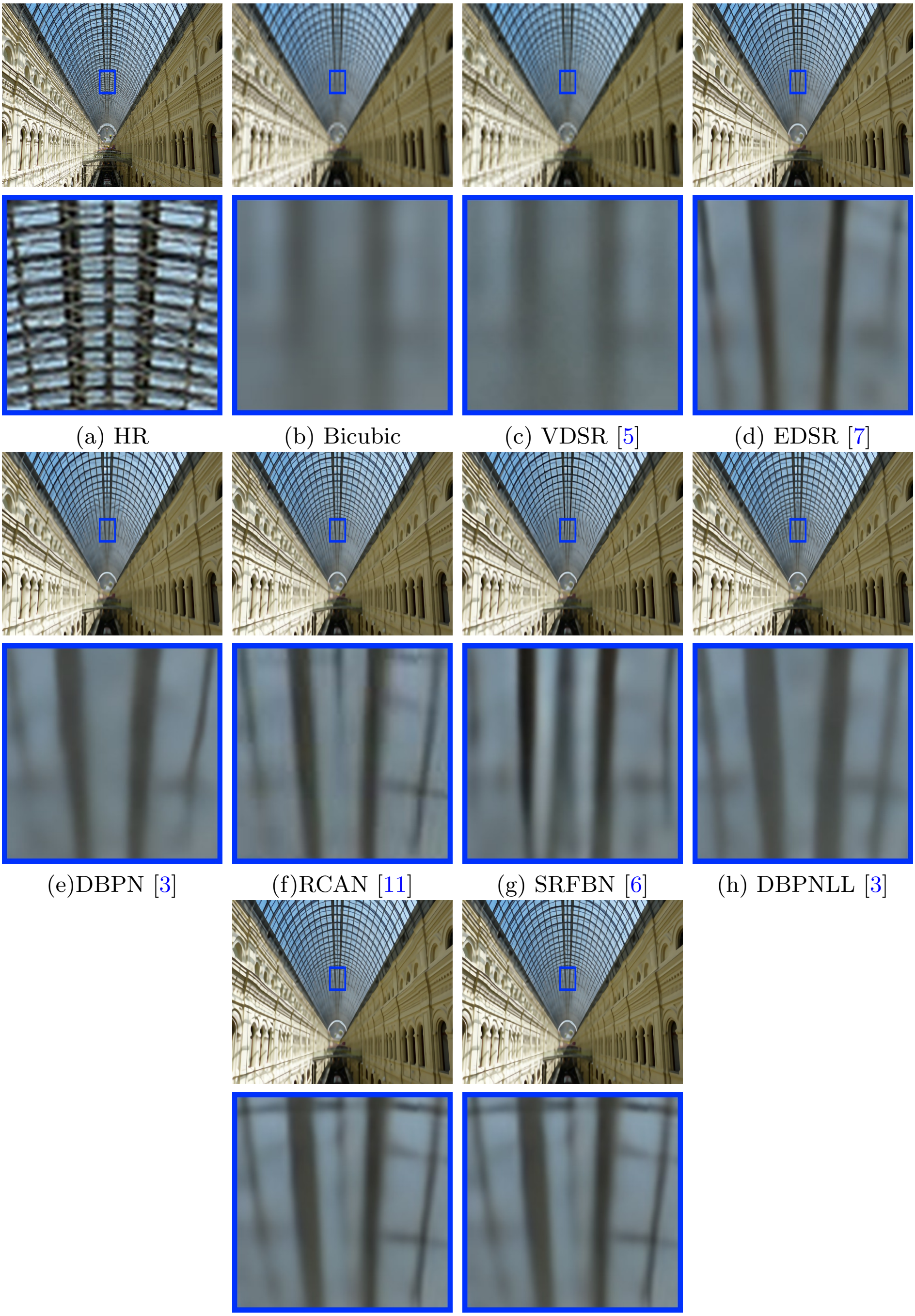

(a) HR (b) Bicubic (c) VDSR [5] (d) EDSR [7]

(e)DBPN [3] (f)RCAN [11] (g) SRFBN [6] (h) DBPNLL [3]

(i) HAN(our) (j) HAN+(our)

Fig. 28. Visual comparison for 8× SR on the Urban100 dataset

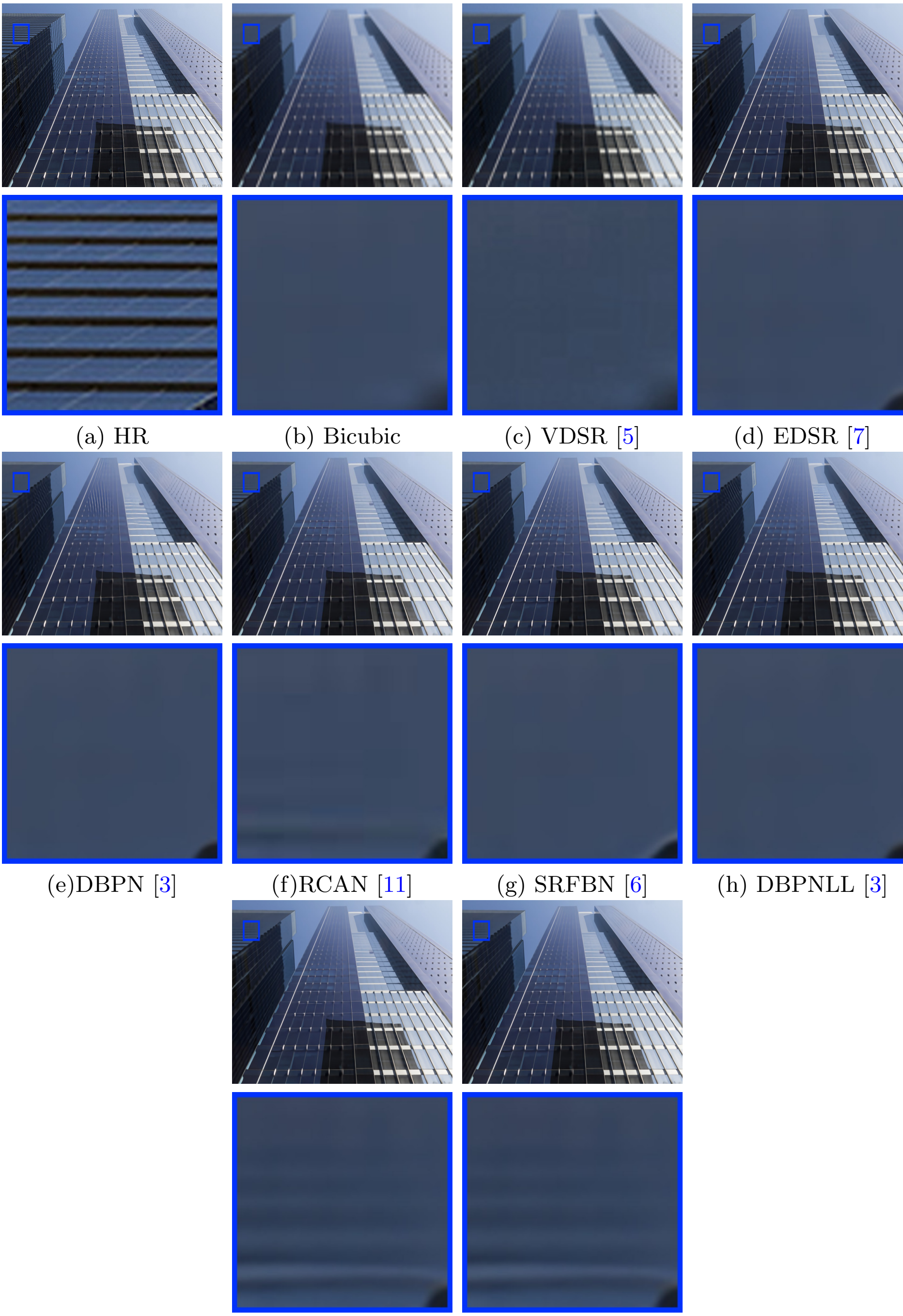

(a) HR (b) Bicubic (c) VDSR [5] (d) EDSR [7]

(e)DBPN [3] (f)RCAN [11] (g) SRFBN [6] (h) DBPNLL [3]

(i) HAN(our) (j) HAN+(our)

Fig. 29. Visual comparison for 8× SR on the Urban100 dataset

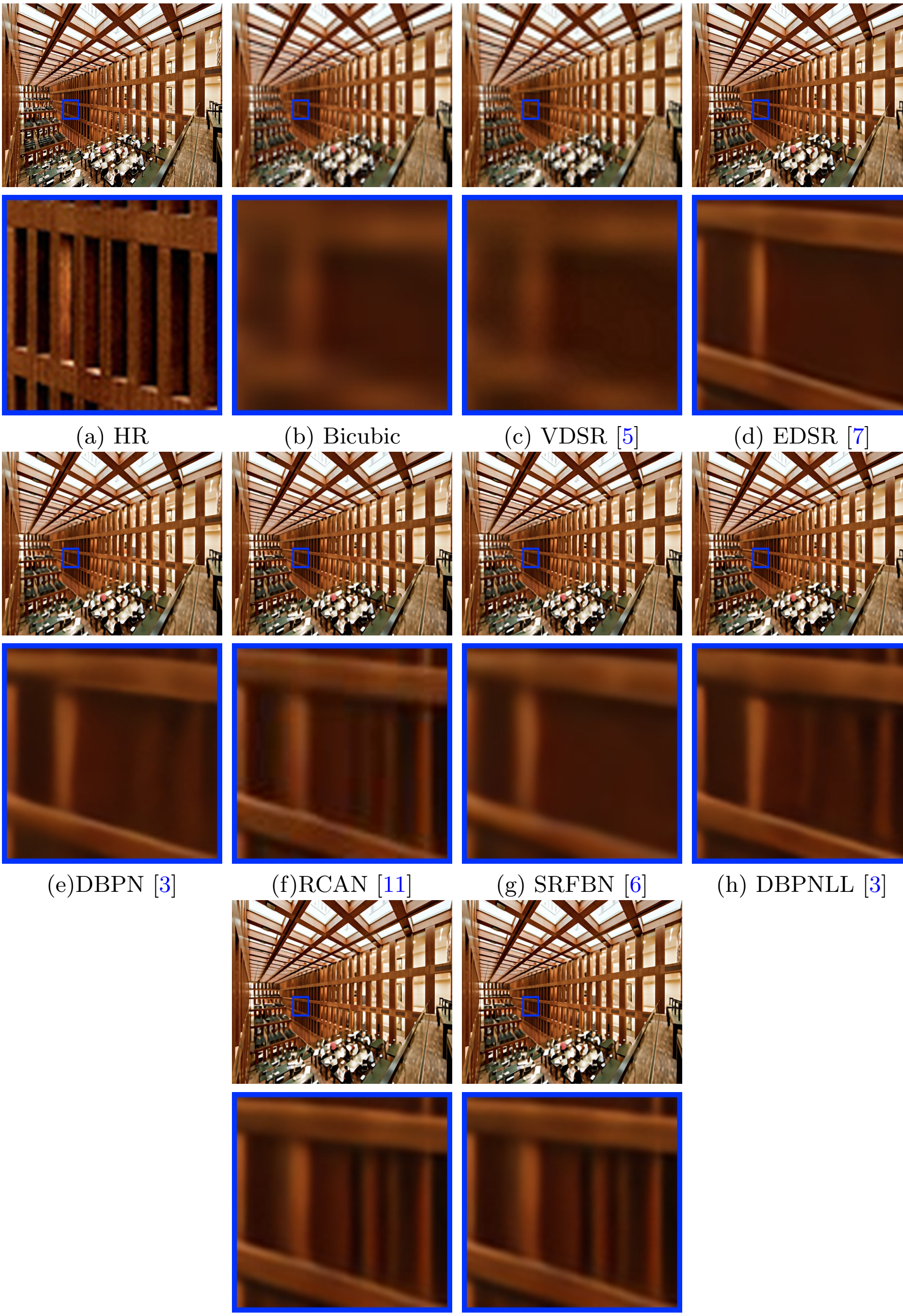

(a) HR (b) Bicubic (c) VDSR [5] (d) EDSR [7]

(e)DBPN [3] (f)RCAN [11] (g) SRFBN [6] (h) DBPNLL [3]

(i) HAN(our) (j) HAN+(our)

Fig. 30. Visual comparison for $8\times$ SR on the Urban100 dataset

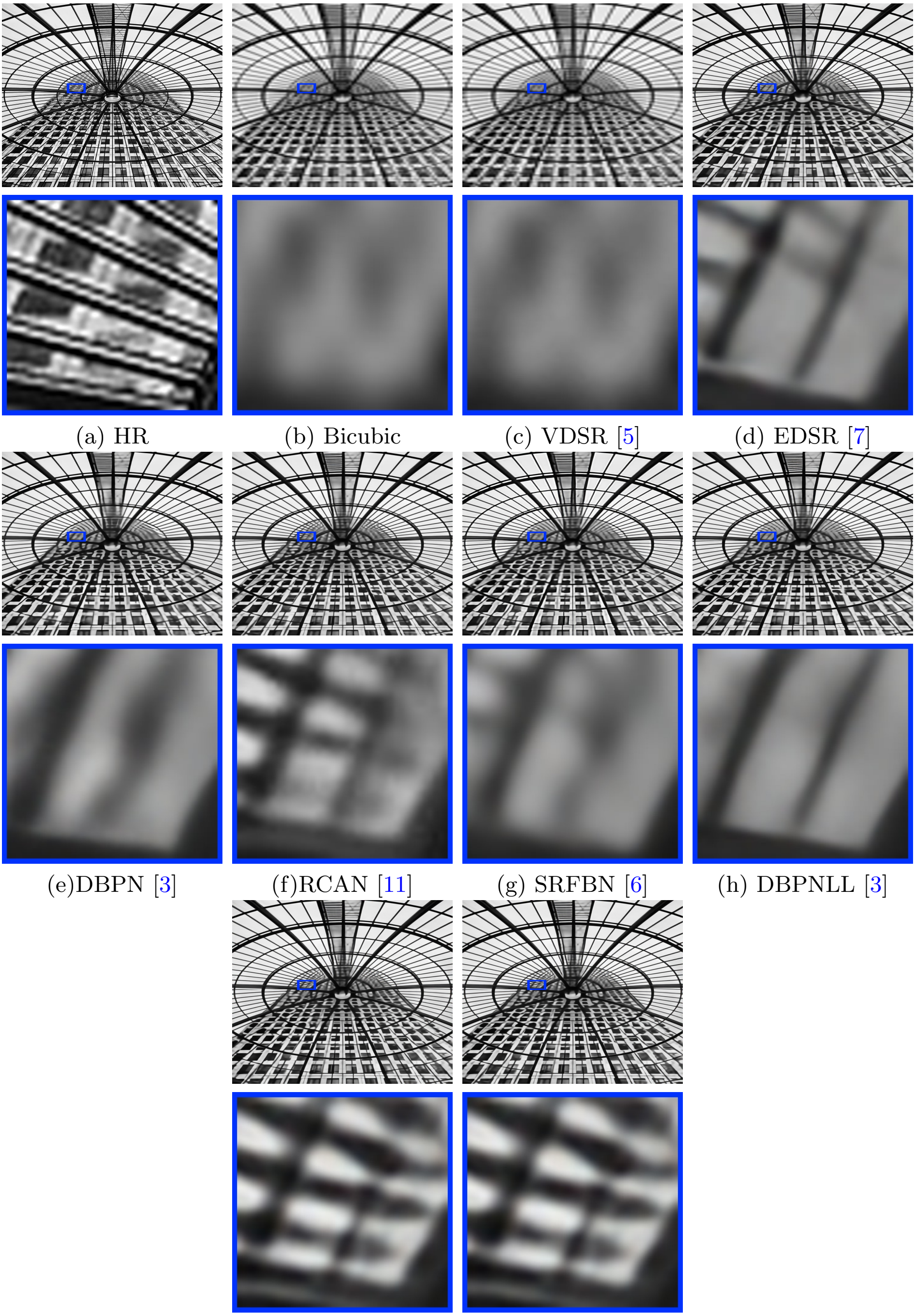

(a) HR (b) Bicubic (c) VDSR [5] (d) EDSR [7]

(e)DBPN [3] (f)RCAN [11] (g) SRFBN [6] (h) DBPNLL [3]

(i) HAN(our) (j) HAN+(our)

Fig. 31. Visual comparison for 8× SR on the Urban100 dataset

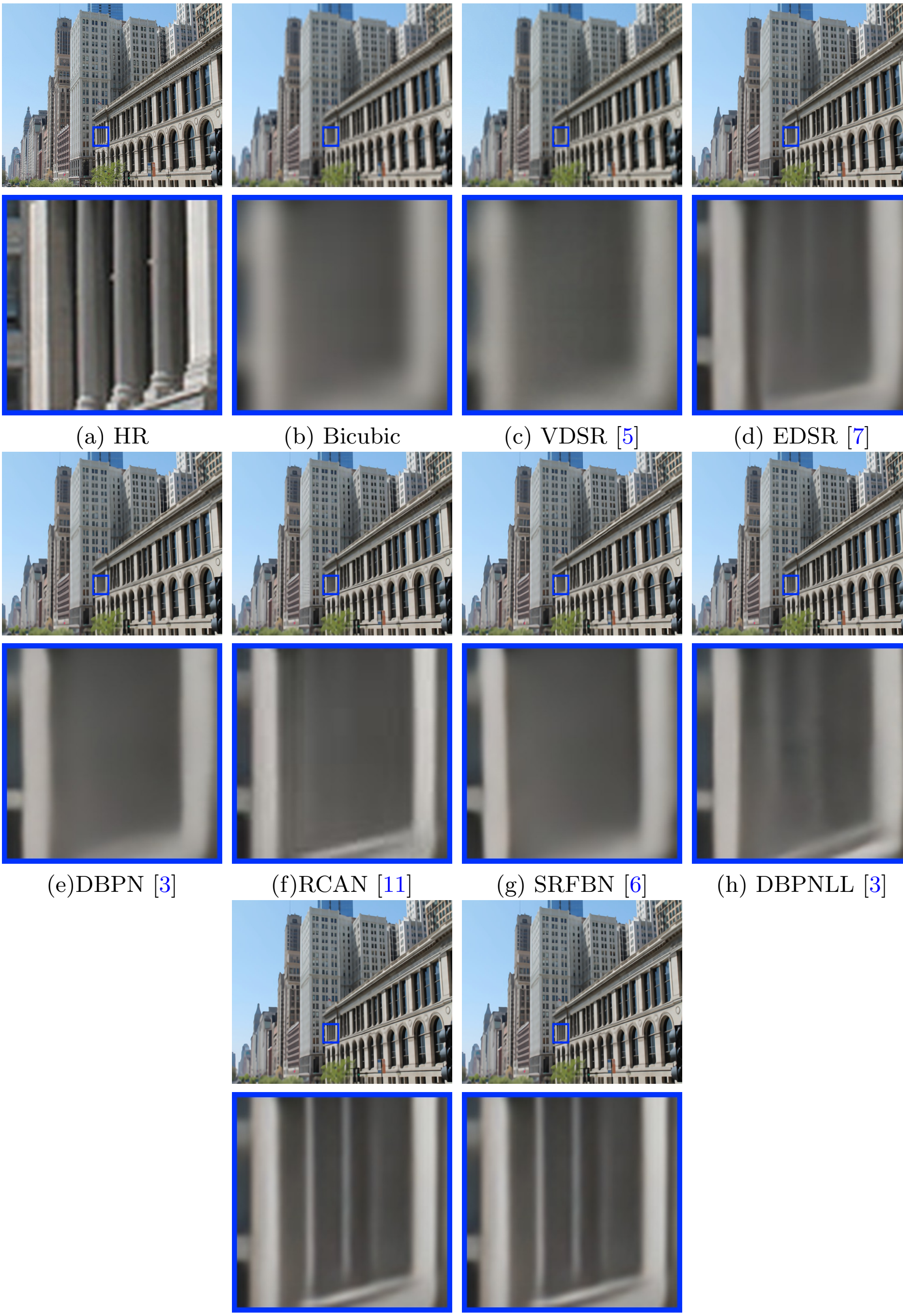

(a) HR (b) Bicubic (c) VDSR [5] (d) EDSR [7]

(e)DBPN [3] (f)RCAN [11] (g) SRFBN [6] (h) DBPNLL [3]

(i) HAN(our) (j) HAN+(our)

Fig. 32. Visual comparison for 8× SR on the Urban100 dataset

(a) Bicubic (b) EDSR [7] (c)RDN [12]

(d)RCAN [11] (e) SRFBN [6] (f) HAN(our)

(g) HAN+(our)

Fig. 33. Visual comparison for real image super-resolution

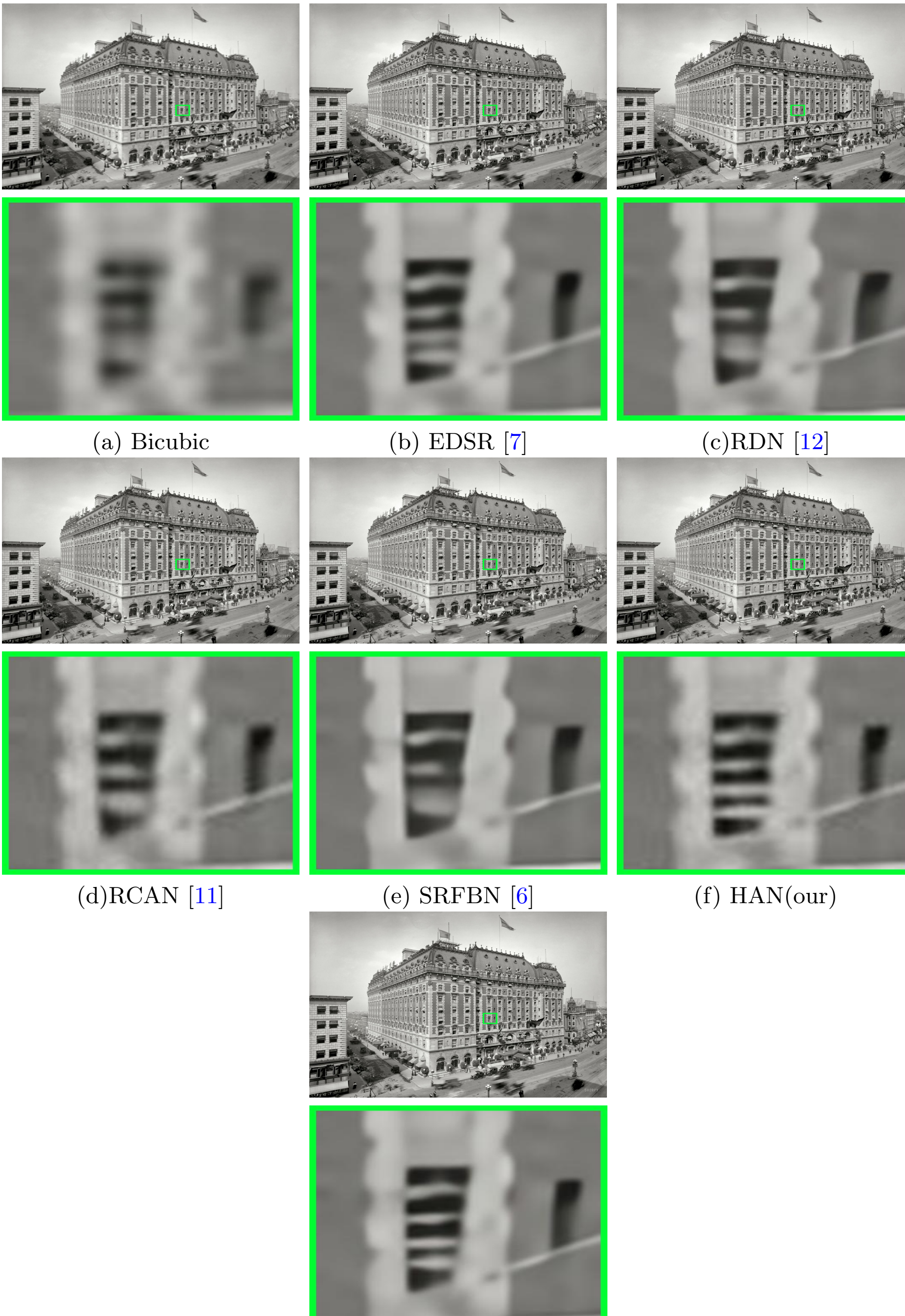

(a) Bicubic (b) EDSR [7] (c)RDN [12]

(d)RCAN [11] (e) SRFBN [6] (f) HAN(our)

(g) HAN+(our)

Fig. 34. Visual comparison for 4× SR on real-world images

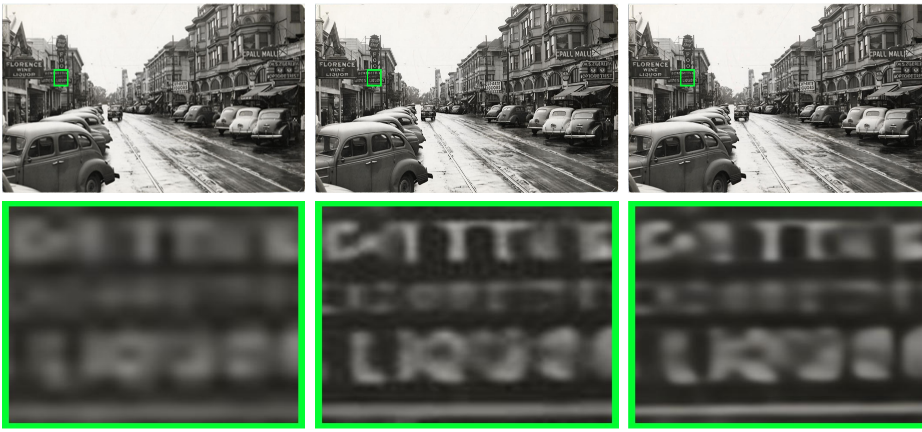

(a) Bicubic (b) EDSR [7] (c)RDN [12]

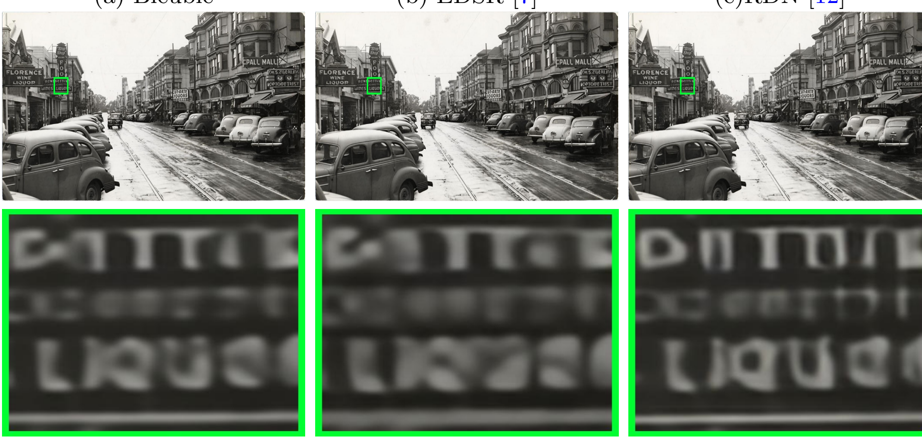

(d)RCAN [11] (e) SRFBN [6] (f) HAN(our)

(g) HAN+(our)

Fig. 35. Visual comparison for 4× SR on real-world images

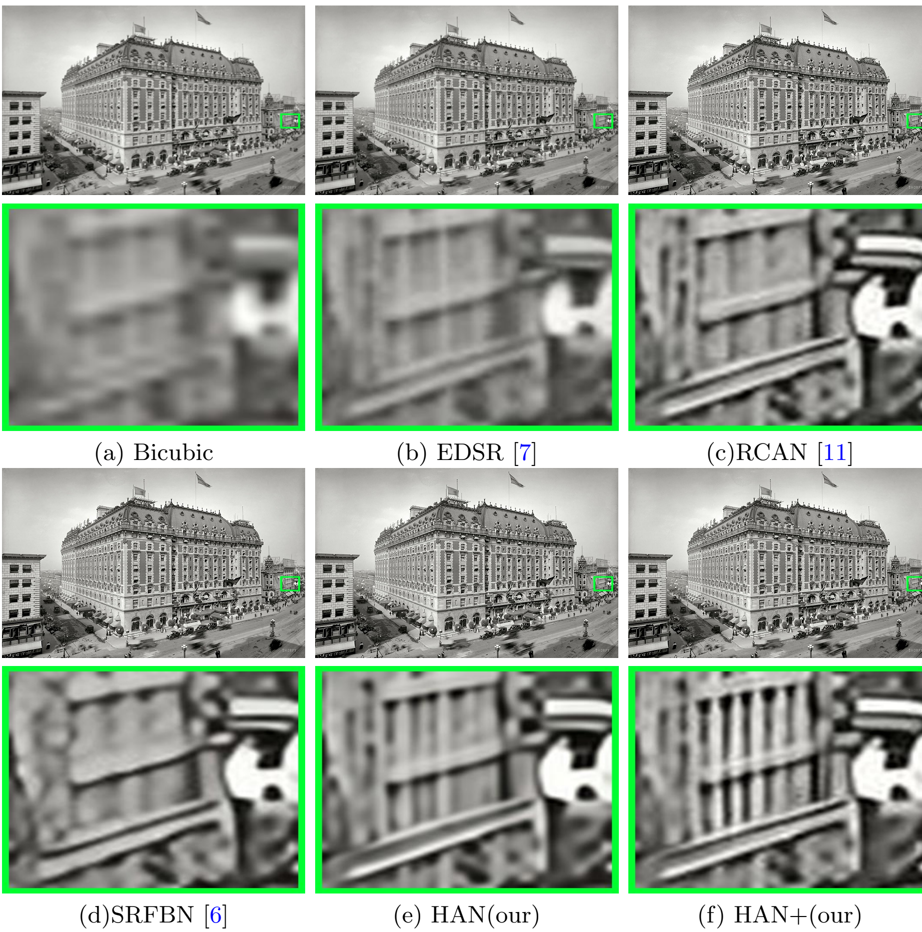

Fig. 36. Visual comparison for 3× SR with BD degradation model on real-world images

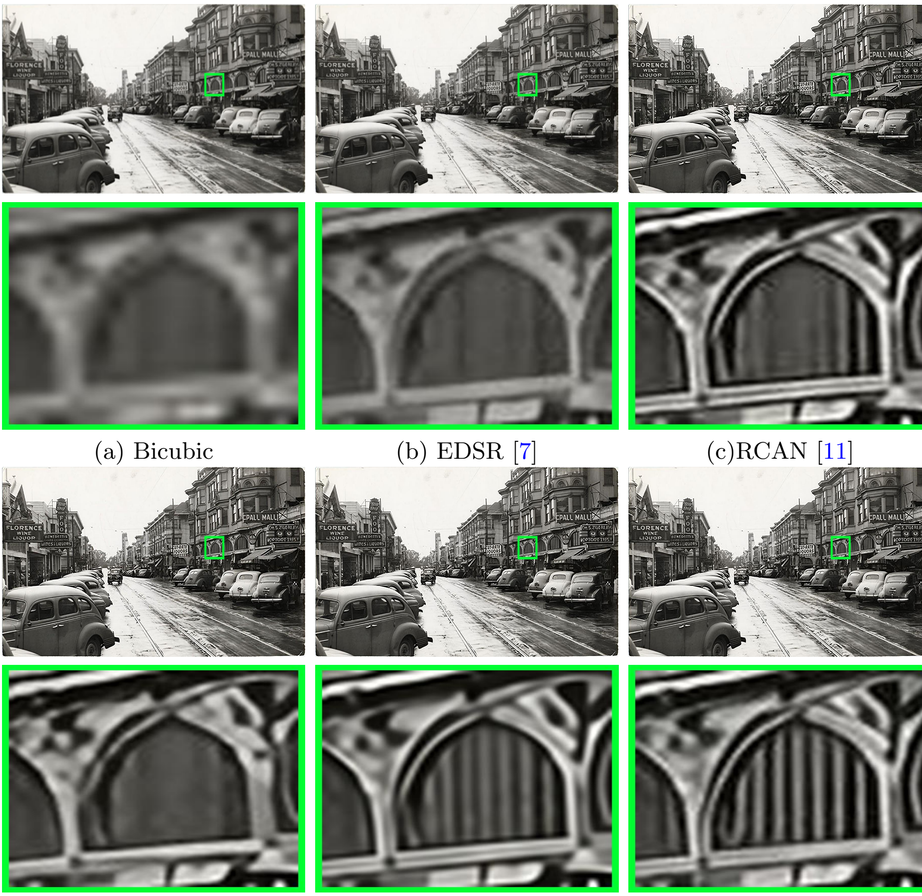

(a) Bicubic (b) EDSR [7] (c)RCAN [11]

(d)SRFBN [6] (e) HAN(our) (f) HAN+(our)

Fig. 37. Visual comparison for 3× SR with BD degradation model on real-world images

References

1. Bevilacqua, M., Roumy, A., Guillemot, C., Alberi-Morel, M.L.: Low-complexity single-image super-resolution based on nonnegative neighbor embedding. British Machine Vision Conference (2012)
2. Dai, T., Cai, J., Zhang, Y., Xia, S.T., Zhang, L.: Second-order attention network for single image super-resolution. In: CVPR. pp. 11065–11074 (2019)
3. Haris, M., Shakhnarovich, G., Ukita, N.: Deep back-projection networks for super-resolution. In: Proceedings of the IEEE conference on computer vision and pattern recognition. pp. 1664–1673 (2018)
4. Huang, J.B., Singh, A., Ahuja, N.: Single image super-resolution from transformed self-exemplars. In: CVPR. pp. 5197–5206 (2015)
5. Kim, J., Kwon Lee, J., Mu Lee, K.: Accurate image super-resolution using very deep convolutional networks. In: CVPR. pp. 1646–1654 (2016)
6. Li, Z., Yang, J., Liu, Z., Yang, X., Jeon, G., Wu, W.: Feedback network for image super-resolution. In: CVPR. pp. 3867–3876 (2019)
7. Lim, B., Son, S., Kim, H., Nah, S., Mu Lee, K.: Enhanced deep residual networks for single image super-resolution. In: CVPR. pp. 136–144 (2017)
8. Martin, D., Fowlkes, C., Tal, D., Malik, J.: A database of human segmented natural images and its application to evaluating segmentation algorithms and measuring ecological statistics. In: ICCV. vol. 2, pp. 416–423 (2001)
9. Matsui, Y., Ito, K., Aramaki, Y., Fujimoto, A., Ogawa, T., Yamasaki, T., Aizawa, K.: Sketch-based manga retrieval using manga109 dataset. Multimedia Tools and Applications **76**(20), 21811–21838 (2017)
10. Zeyde, R., Elad, M., Protter, M.: On single image scale-up using sparse-representations. In: International conference on curves and surfaces. pp. 711–730 (2010)
11. Zhang, Y., Li, K., Li, K., Wang, L., Zhong, B., Fu, Y.: Image super-resolution using very deep residual channel attention networks. In: ECCV. pp. 286–301 (2018)
12. Zhang, Y., Tian, Y., Kong, Y., Zhong, B., Fu, Y.: Residual dense network for image super-resolution. In: CVPR. pp. 2472–2481 (2018)